INVESTIGATING THE EFFECT OF BALL IMPACT LOCATION ON THE OVERHEAD MOTION IN TENNIS DURING GAME PLAY

A thesis presented to the faculty of the Graduate School of Western Carolina University in partial fulfillment of the requirements for the degree of Master of Science in Technology.

By

Ainhoa Iglesias Díaz

Director: Martin L. Tanaka, PhD
Assistant Professor
Department of Engineering and Technology

Committee Members:
Aaron K. Ball, PhD
Department of Engineering and Technology
Paul M. Yanik, PhD
Department of Engineering and Technology

April 2014

In dedication to my greatgrandmother,
Toribia.
Thank you for guiding me from heaven.
You give me the strength to keep going.
I hope one day you can be as proud of
me as I am of you.

I love you.

ACKNOWLEDGEMENTS

I would like to thank everyone who has contributed to my research in one way or another. This thesis has been a difficult and interesting adventure that has taught me much more than I expected. It is from failures that we learn the most.

I would like to thank my thesis director, Dr. Martin Tanaka, and my committee members, Dr. Paul Yanik and Dr. Aaron Ball, for their assistance, support and guidance. In addition, I would like to express my sincere gratitude to Western Carolina University and especially to The Kimmel School for giving me the opportunity to come from overseas to pursue my education. To my classmates and friends who encouraged and helped me out when I needed it, I thank you all.

Commitment, effort, and dedication were fundamental elements for the completion of my thesis, but even more was the support of my family. I would like to thank my parents, Francisco and Yolanda, my sister Nadia, and my grandmother Rosa. Thank you for working so hard all your life to provide me with such a great life and giving me the opportunity to make my dreams come true. Thank you for your endless support. Thank you for being there and believing in me. Thank you for teaching me that there is no other path to achieve your goals but hard work. Thank you so much for pushing me to work even harder when I could not see the light. Words can't describe how grateful I am to all of you. I could not have made it to where I am, and become the person I am today without you.

"Opportunities to find deeper powers within ourselves come when life seems most challenging." - Joseph Campbell

TABLE OF CONTENTS

LIST OF TABLES

LIST OF FIGURES

ABSTRACT

INVESTIGATING THE EFFECT OF BALL IMPACT LOCATION ON THE OVERHEAD MOTION IN TENNIS DURING GAME PLAY

Ainhoa Iglesias Díaz, M.S.T.

Western Carolina University (April 2014)

Director: Martin L. Tanaka, PhD

Tennis is a competitive sport played by millions of people worldwide. The characteristics of the game of tennis produce stress on the musculoskeletal system, especially in the upper extremity. Upper extremity injuries often occur when the arm is highly accelerated, as happens in tennis. These high accelerations require large forces to be applied to the wrist, elbow and shoulder. Upon ball impact, a large amount of force is transferred to the ball from the tennis racket. However, depending on the impact location, large reaction forces can also be produced in the body. These large reaction forces must pass through the kinematic chain from the hand to the wrist, elbow and shoulder joints and into the torso. As a result, wrist, elbow and shoulder joint injuries are common. Motion capture has been used to study the biomechanics of the overhead motion in tennis; yet, this method measures pre- and post-impact dynamics not the actual instant at which the interaction between the ball and the racket occurs. Therefore, to make a more accurate representation, the impact itself needs to be studied. Investigating the impact itself will provide more insight into what is happening at the exact moment of the collision and how the kinematic chain is affected.

A commercial racket was purchased and customized by substituting the original handle by a one inch diameter acetyl rod, and adding unidirectional and triaxial strain gauges to it. A custom electrical circuit was designed and built to measure the strain in the racket handle during ball impact. Two participants used the instru-

mented racket to each hit a total of 20 regular serves divided into 4 different sets. Participants were photographed during the serve using a high speed camera at 120 frames per second. These photographs were used to identify the ball impact location of each serve. Strain waveforms collected using a custom electrical circuit were analyzed to determine the peak ball impact force, the wrist reaction forces, and torques from the bending moments developed in the racket handle during impact.

Results showed that the instrumented tennis racket was able to evaluate the effect of ball impact location of the overhead motion in tennis during game play. The instrumented racket was able to measure ball forces, wrist reaction forces (equal in magnitude to ball forces but opposite in direction as a result of not taking into account the transfer of linear and angular momentums) and torques generated by the bending moments at the hand during ball impact.

This device or an improved version may be useful to get a better understanding of the forces and moments created with different types of movements during tennis play. It would be especially useful when employed in collaboration with a motion capture system. A more complete understanding of tennis biomechanics can be gained by including racket impact forces and bending moments with motion capture to quantify the effect that ball impact location has on the transfer of forces to the joints passing through the kinematic chain.

CHAPTER 1: INTRODUCTION

Tennis is a competitive sport played by millions of people worldwide [1]. A large number of injuries are associated with sports. Sipes and Laudner [2] documented that 30% of collegiate athletes have had shoulder injuries during their athletic careers. Like most sports, tennis requires a certain level of technique to avoid movements that can cause injuries.

The characteristics of the game of tennis produce stress in the musculoskeletal system, especially in the upper extremity. Upper extremity injuries often occur when the arm is highly accelerated, as happens in tennis. These high accelerations require large forces to be applied to the wrist, elbow and shoulder. Upon ball impact, a large amount of force is transferred to the ball from the tennis racket. However, depending on the impact location, large reaction forces can also be produced. These large reaction forces must pass through the kinematic chain from the hand to the wrist, elbow and shoulder joints and into the torso. As a result, wrist, elbow and shoulder joint injuries are common in tennis.

In order to prevent injuries, it is necessary not only to study the biomechanics of the overhead motion in tennis but also the effect of ball impact location during game play. The ideal location of impact depends not only on the center of mass of the tennis racket, but also upon the angular momentum of the racket upon impact. Ball speed after impact results from the transfer of both linear momentum and the rotational energy from the racket to the ball. Joint reaction forces result from less than ideal momentum transfer to the ball which can cause joint stress and overuse injuries.

Motion capture using marker based systems is the most common method used to study the overhead motion in tennis [3]. This technology utilizes retro-reflective

markers placed on the surface of the skin and multiple video cameras to capture and track the position of the body segments over time. The downside is that skin movement can cause the marker location to move with respect to the body segment which can lead to inaccuracies. However, all the studies using this method focus on pre- and post-impact dynamics. They look at the motion as a whole rather than looking at what happens right at the moment when the collision between the racket and the ball occurs. To obtain a more accurate representation, the impact itself needs to be studied. Evaluating the impact itself will provide more insight into what is happening at the exact moment of the collision and how the kinematic chain is affected. Hence, a more complete understanding can be gained by including racket impact forces and bending moments at impact along with motion capture to quantify the effect that ball impact location has on the transfer of forces to the joints passing through the kinematic chain.

Instrumentation on the tennis racket can be used to directly measure impact parameters and provide more accurate data corresponding to the ball impact. Accelerometers and strain gauges have been used to measure accelerations and forces during ball impact [4]. However, previous research efforts have used a stationary test configuration with the tennis racket firmly fixed to the rigid structure. None of these studies investigate forces generated while the tennis racket is moving.

This research evaluated the wrist reaction forces and moments generated at the tennis racket grip while performing the overhead motion. Unlike previous studies the impact forces were measured directly and during actual game play. In order to obtain these data, an instrumented tennis racket was developed that included a custom racket handle, unidirectional and triaxial strain gauges, and a custom Wheatstone bridge circuit with amplification and signal conditioning. The instrumented tennis racket was integrated with a high speed oscilloscope and a personal computer to create the data acquisition system used for the study.

The focus of this research was to investigate the effect of ball impact location when performing the overhead motion during game play. Although the major goals were achieved, there were limitations to the study. The instrumented racket was heavier than a regular tennis racket due to the new materials added for the purpose of the experiment. Angular and linear momentum were not taken into account because 3D motion capture equipment was unavailable to track motion during the swing. Evaluation of the ball impact location was limited to the y-direction. Finally, a large number of hits by a small number of people were used to obtain consistent results, however as a consequence this limits the information that can be obtained about differences between populations. Overall this new system was able to determine the wrist reaction forces and torques from the bending moments developed in the racket handle at ball impact during actual game play.

CHAPTER 2: LITERATURE REVIEW

2.1 Shoulder Anatomy

The shoulder is composed of three bones: the clavicle, humerus and scapula (Figure 2.1). The clavicle or collarbone holds the shoulder to the body. The humerus or upper arm bone is covered by the articular cartilage and gives the shoulder a wide range of motion but also makes it vulnerable to injury. The scapula or shoulder blade is the bone that connects the humerus with the clavicle. The scapula extends up and around the shoulder joint to form the acromion (top back part) and around the shoulder at the front part of the shoulder blade to form the coracoid process [5, 6].

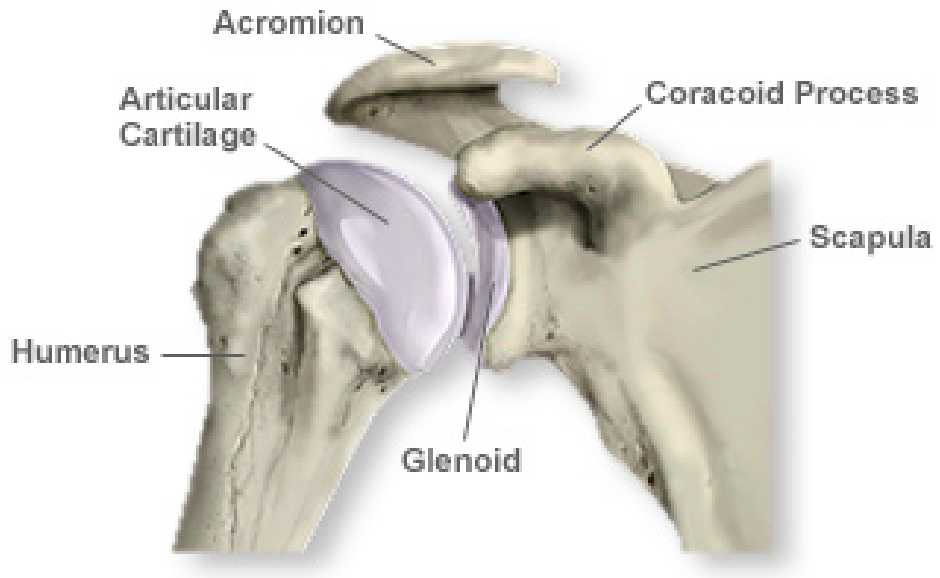

Figure 2.1: Shoulder anatomy [5]

Of the four shoulder joints (sternoclavicular, acromioclavicular, glenohumeral and scapulothoracic), the glenohumeral joint is the one responsible for the majority of arm movement. It consists of a ball-and-socket synovial joint that connects the humerus, the large bone in the upper arm, to the shoulder complex. This joint permits the large range of motion associated with the shoulder. However, this large

range of motion also makes the shoulder joint less stable. The glenohumeral joint is surrounded by a soft tissue called the joint capsule [7]. The coracohumeral ligament and three glenohumeral ligaments connect the humerus to the bones of the shoulder. Tendons join the muscles to the surrounding bones. The biceps tendons (long head and short head of biceps) connect the biceps muscle to the bones of the shoulder and help the biceps flex the forearm. The supraspinatus tendon connects supraspinatus muscle to the top of the humerus [5–7].

The rotator cuff is a musculotendinous complex that stabilizes the shoulder (Figure 2.2). It consists of four tendons that connect the deepest layer of muscles to the humerus. The muscles are subscapularis, supraspinatus, infraspinatus and teres minor. The supraspinatus tendon is the most commonly affected by overuse (subacromial impingement) and trauma/injury (rotator cuff tear). A sac of fluid, the bursa, protects the tendons of the rotator cuff [5–7].

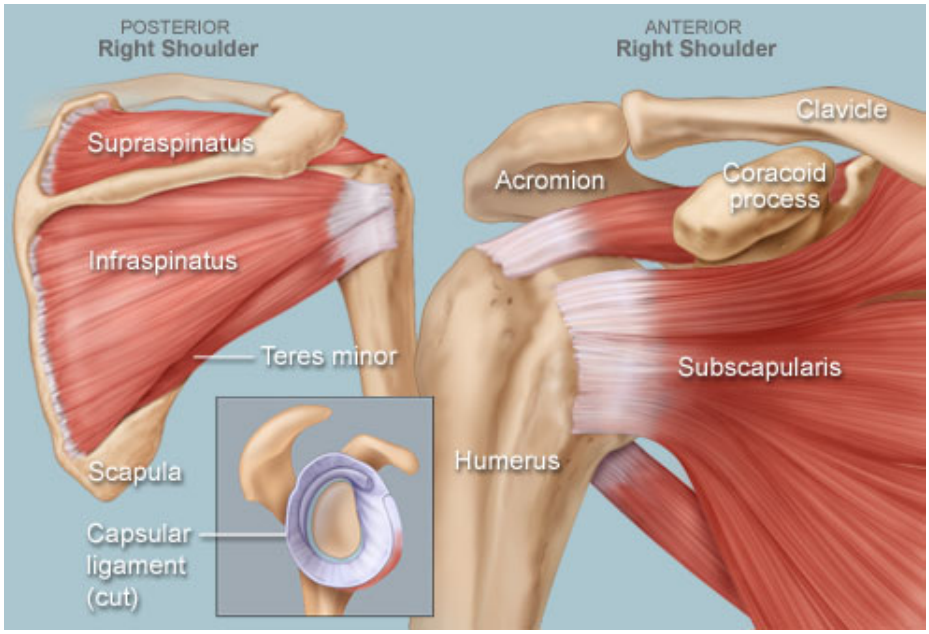

Figure 2.2: Rotator cuff muscles [8]

2.2 Range of Motion

The three planes that define the range of motion of a human body are the sagittal, frontal, and transverse planes (Figure 2.3). The sagittal plane is the vertical that divides the body into right and left sections. The frontal or lateral divides the body into a front and back sections. The transverse or horizontal plane divides the body into an upper and lower section. Because each part of the body was designed to move in a specific way, the importance of maintaining the full range of each joint is desirable for optimal physical health to avoid injuries.

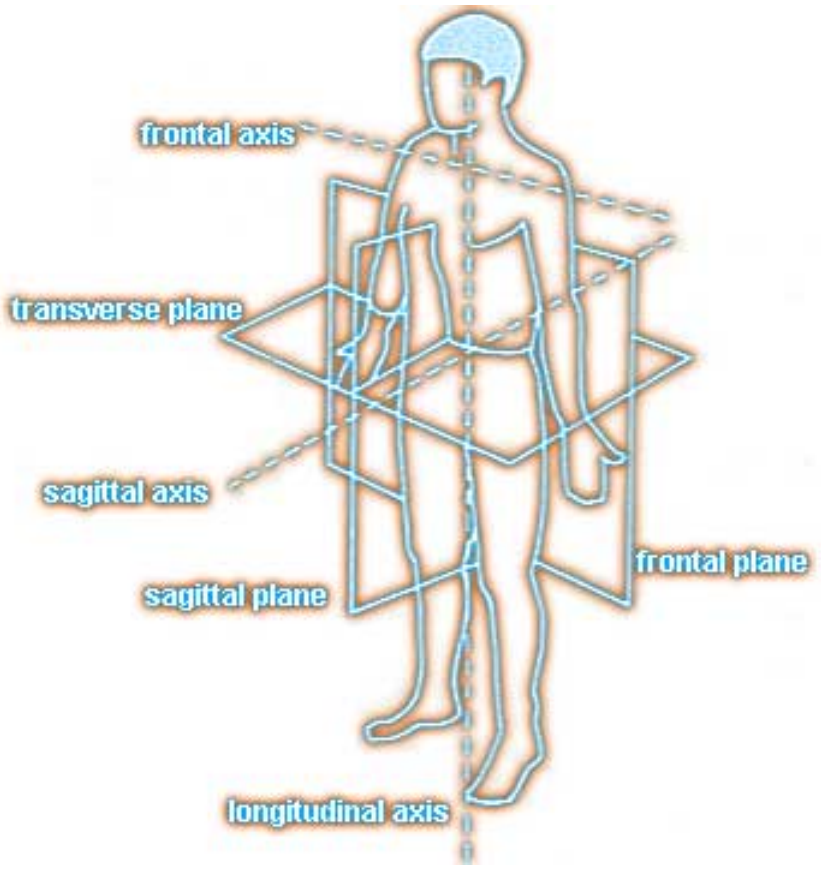

Figure 2.3: Body planes [8]

2.3 Shoulder Injuries in Tennis

The mechanism of the overhead action in throwing sports has been studied because of its importance and relevance to sports performance [9]. Compared to other motions, the throwing motion is quite unnatural to the body, and often moves the arm beyond the joints normal range of motion. Good kinematic chain function (the system formed by the segments that go from the hand to the wrist, from the wrist to the elbow, and from the elbow to the shoulder), good stability and coordination of the scapula are extremely important when performing the overhead action. Hoeven and Kibler [10] state that the rotator cuff muscles and capsular structure are key elements for the stability of the center of rotation during the overhead motion. Playing tennis can cause a variety of shoulder injuries that result from the specific physiologic and mechanical stresses to the musculoskeletal system [11].

Most shoulder injuries in tennis players are classified as overuse and involve the rotator cuff or biceps tendon, or both, according to Neer [12]. Ellenbecker, Roetert and Safran [11] explain that this is due to the overhead nature of the tennis serve where the rotator cuff and biceps tendon can be placed in a compromised position between the humeral head and coracoacromial arch which results in subacromial impingement. Edwards, Bell and Bigliani [13] point out the necessity of further investigation of these lesions since there has been much controversy on the pathology of them.

GIRD or Glenohumeral Internal Rotation Deficit is defined as the loss in degrees of glenohumeral internal rotation of the throwing shoulder compare to the non-throwing shoulder [10]. That is, there is an increase in external rotation and a decrease in internal rotation. This deficit occurs when there is a decrease in rotational arc produced when the limitation of internal rotation exceeds the gain in external rotation. When this happens, the external rotation caused by the abduction of the arm shifts the humeral head to a more posterosuperior location, which results in impingement of the rotator cuff and bursa between the humeral head and acromion [14]. Later

on, this was supported by Burkhart, Morgan, and Kibler [15]. Also, Walch et al. [16] say that it is the 90 degree position of glenohumeral joint abduction with humeral rotation that can cause the direct contact between the undersurface of the rotator cuff and the posterior labrum and glenoid, which also results in posterior or undersurface impingement. This kind of injury can be exacerbated by anterior glenohumeral joint instability. The anterior instability of the glenohumeral joint can be caused by insufficiency of the static (inferior glenohumeral ligament and anterior inferior glenoid labrum) and dynamic (rotator cuff complex) stabilizers [17].

SLAP or Superior Labrum Anterior-Posterior lesions of the shoulder are very common in tennis players as well. This injury consists of a tear in the superior glenoid labrum that it is located near the attachment of the long head of the biceps brachii tendon [18]. SLAP lesions have an effect on the glenohumeral rotation and translation. There are two leading theories of possible causes: posterior shoulder tightness: posterosuperior humeral head translation leads to a peeling off of the posterosuperior labrum [15]; and repeated external and internal rotation of the shoulder, and thus the biceps tendon, with applied tension leads to the superior labrum pulling off the glenoid [18]. There is a close relation between SLAP and GIRD lesions and instability. Usually, the increase in anterior translation is a consequence of a SLAP lesion [10]. Panossian and colleagues [19] present a study in which they compare changes in humeral rotation range of motion and glenohumeral translation after the creation of a SLAP lesion.

Posterior capsular tightness has been found in infraspinatus atrophy due to suprascapular nerve injury. The suprascapular nerve can get injured especially as it passes through the spinoglenoid notch [11]. One of the possible causes is when the spinoglenoid ligament inserts into the posterior glenohumeral capsule, causing compression of the suprascapular nerve as it passes around the spine of scapula [20].

PASTA or Partial Articular Supraspinatus Tendon Avulsion lesions are a variety of the Partial-thickness rotator cuff tears (PTRCTs) which, according to Snyder and Bond [21], are the most common form of rotator cuff injury. This injury is a partial tear in one of the rotator cuff tendons of the shoulder: the supraspinatus, which stabilizes the arm at the shoulder. The natural history of PASTA lesions is not completely understood and there is no specific cause (intrinsic, extrinsic and traumatic), but it is considered more a lack of vascularity rather than impingement syndrome.

TOS or Thoracic outlet syndrome is caused by pressure on the trunks and medial cord of the brachial plexus, the subclavian artery, or the subclavian vein [6]. The incidence of this injury is increased in athletes who perform repetitive overhead movements. TOS may occur due to a positional cause, for example, by abnormal compression from the clavicle (collarbone) and shoulder girdle on arm movement. According to the National Institute of Neurological Disorders and Stroke [22], TOS is an umbrella term that encompasses three related syndromes that involve compression of the nerves, arteries, and veins in the lower neck and upper chest area and cause pain in the arm, shoulder, and neck.

2.4 Studies of Joint Mechanics in relation to injuries

Overuse injuries, such as the ones mentioned in the previous section, can result from various risk factors such as gender, age, repetition, and excessive joint loadings [23]. There have been many studies on the overhead motion in tennis. Martin et al. [24] compared the joint kinetics and stroke production efficiency for the shoulder, elbow, and wrist during the serve between professionals and advanced tennis players, and concluded that advanced tennis players were at a higher risk of shoulder and elbow injuries than professional players because they were unable to maximize ball velocity with lower joint kinetics. Elliott et al. [25] also showed how variation in serve techniques loaded the shoulder joint differently, which could have implications for

injuries. Professional tennis players were able to have a more consistent and regular motion throughout the game than advanced players and, therefore, they were able to minimize the risk of injuries.

Understanding the effect of impact location on the transfer of linear and angular momentum to a tennis ball during game play is fundamental to understanding the biomechanics of shoulder injuries. Bahamonde [26] studied the changes in angular momentum during the tennis serve using a three-dimensional cinematography and direct linear transformation method. Other research has used motion capture system with reflective markers to study the differences of momentum transfer from the trunk to upper extremities and to the racket for different stances and player skill level [27].

To summarize, there have been various studies on the mechanics of the overhead motion in tennis where the focus is on different variables such as position of the legs, stroke efficiency, different serve techniques (flat, kick, slice), and transfer of momentum. These are important aspects; however, these studies focus on pre and post impact dynamics to investigate the motion as a whole and to indirectly determine what happens at the moment when the collision between the racket and the ball occurs.

2.5 Motion Capture Methods

Marker based motion capture is considered the gold standard for motion capture. It has been used extensively to study various types of human movement including gait, running, baseball, and tennis [3]. This technology utilizes retroflective markers placed on the surface of the skin to capture the linear and angular position of body segments. Multiple video cameras are used to triangulate the location of each marker and track its movement over time. This technology is capable of locating a marker in 3D space with an accuracy of 1 mm. However, there are concerns with using this technology. Skin movement can cause the marker location to move with

respect to the body segment leading to inaccuracies [28]. Gordon and Dapena [29] also found differences in the twist angles along the limb when measured with skin markers versus vectors passing through upper limb centers of the joint. It has also been proposed that the use of markers may require players to change the mechanics of the serve motion [3]. However, despite these concerns, marker-bases systems are still used in motion capture and new techniques are being developed where distinguishable markers are placed on the human body [30].

Motion capture is capable of estimating forces and moments at impact by comparing the differences in the linear and angular velocities of the body segments., However, it is only an indirect measure of forces and moments and the errors wit motion capture stated above will result in errors in the calculated forced and moments. Actual impact dynamics result in forces and moments that affect the wrist, elbow and shoulder joint differently which can consequently cause the overuse injuries described in previous sections.

2.6 Accelerometry: a technique for measuring movement and patterns

The motion capture systems described in the previous section are expensing, often exceeding $250,000 USD. An alternative way to measure motion is using an accelerometer. An accelerometer is an electromechanical device used to measure acceleration forces. Such forces may be static, like the continuous force of gravity or, as is the case with many mobile devices, dynamic to sense movement or vibrations. The force caused by vibration or a change in motion (acceleration) causes the mass to "squeeze" the piezoelectric material which produces an electrical charge that is proportional to the force exerted upon it. Since the charge is proportional to the force, and the mass is a constant, then the charge is also proportional to the acceleration [31, 32].

Accelerometers have been used for several decades to monitor body movement in subjects [33] as well as to determine posture and patterns especially during walking and running. Using accelerometers attached to the body to measure segmental accelerations during walking enables tests to be easily performed outside the laboratory environment [34] and it allows continuous monitoring of movement, suitable for patients with chronic diseases [31].

In tennis, accelerometers have been used to investigate the translational and rotational motion of the swing to identify the correlation between the skill level and the characteristics of the first serve swing [35]. However, in these studies the accelerometers were mounted on the knee, leg and wrist. James Savage [4] used a configuration that consisted on a single lightweight accelerometer attached to the tip of the racket frame as well as eight full bridge strain gauges attached to the handle to measure the impact of the ball. This setup enables the magnitude of the strains in the racket handle to be quantified in real time and to describe the times at which reaction forces occur with respect to impact. However, it was a stationary test where the racket was clamped to a table and the ball impact was aligned with the approximate center of the racket head. Aligning the ball impact with the center of the racket head generated an impact allowing for the measurement of both racket vibrations and the bending at the handle of the racket. In important point is that the experiment was not performed during actual game play.

Although there are several studies that use strain gauges attached to the racket we could not find any published papers that investigated forces generated while the tennis racket is moving.

2.7 Strain gauges

Strain gauges are devices used to measure the strain within a material at the location that they are attached. The most common type of strain gauge is the bonded metallic strain gauge which consists of an insulating flexible backing which supports a metallic foil pattern [36, 37]. The foil is a resistor that conducts the electricity. When a tensile load is applied to the surface of the object to which the strain gauge is attached, the object stretches. The foil also stretches making it longer and thinner causing the electrical resistance to increase because the electricity has to travel further through a more constricted path. Compressive loads have the opposite effect. The strain is, therefore, measured in terms of the electrical resistance of the foil wire, which varies linearly with strain [36, 37].

2.8 Wheatstone Bridge and its application for the use of strain gauges

The Wheatstone bridge, named after Sir Charles Wheatstone [38], is a bridge circuit used to measure small changes in resistance and is, therefore often used to measure the resistance change in a strain gauge.

The Wheatstone bridge consists of a dc voltage source, four resistors and a voltmeter to measure voltage output. When the bridge is fully balanced, the resistors on each leg of the bridge will be balanced and the voltage across the bridge will be zero. A voltage difference will appear when the resistance of any of the resistors changes. The Wheatstone bridge is the most common circuit used to measure strain gages [38], where one of the resistors is substituted by a strain gauge.

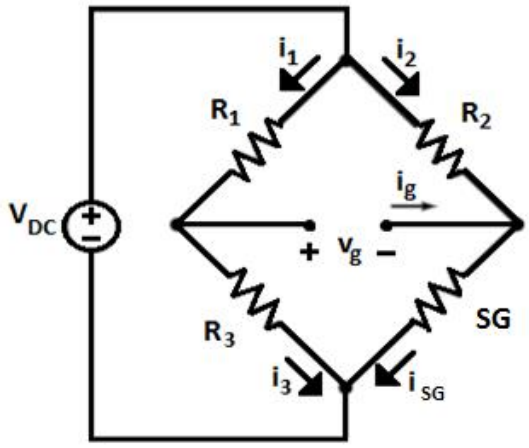

Figure 2.4: Wheatstone Bridge

By applying Kirchhoffs Voltage Law (KVL) to the top of the bridge, voltage across R_1 was found to be equal to the voltage across R_2 when $v_g = 0$.

$$R_2 i_2 - v_g - R_1 i_1 = 0 \longrightarrow R_2 i_2 = R_1 i_1 \tag{2.1}$$

By applying KVL to the bottom part of the bridge, voltage across R_3 was found to be equal to the voltage across R_{SG} when $v_g = 0$.

$$v_g + R_{SG} i_{SG} - R_3 i_3 = 0 \longrightarrow R_3 i_3 = R_{SG} i_{SG} \tag{2.2}$$

By applying Kirchhoffs Current Law (KCL) to each of the nodes, the current through i_1 equals the current through i_3. In the same way, the current through i_2 equals the current through i_{SG}.

$$i_1 = i_3, \quad \text{and} \quad i_2 = i_{SG} \tag{2.3}$$

There are different Wheatstone bridge configurations: quarter bridge (uses only one variable resistor or active strain gage), half bridge (uses two variable resistor or active strain gages in two bridge arms), and full bridge (uses four variable resistors or active strain gages in all four bridge arms) .

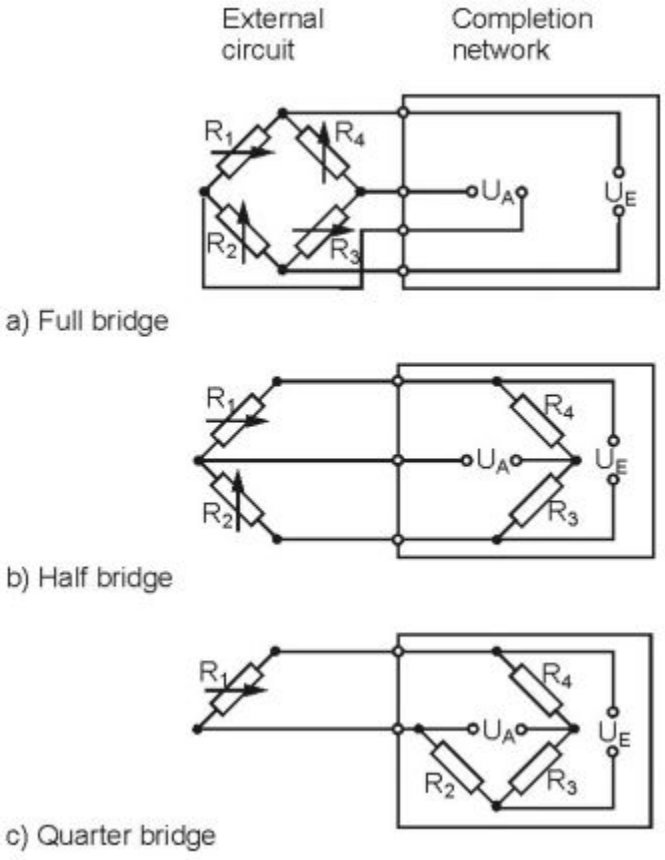

Figure 2.5: Wheatstone Bridge configurations [38]

When using a quarter bridge configuration, R_1,R_2, and R_3 are fixed value resistors and R_{SG} is the resistance of the strain gage that will change with loading. The following equation shows how to calculate the value for R_{SG}

$$R_{SG} = \frac{R_2}{R_1} R_3 \tag{2.4}$$

The voltage out is a function of the input voltage and the four resistors. Voltage out will be proportional to the change in resistance observed in the strain gauge when a load is applied.

$$V_{OUT} = V_{IN}\Big[\frac{R_3}{R_3 + R_S G} - \frac{R_2}{R_2 + R_1}\Big] \tag{2.5}$$

CHAPTER 3: METHODS

3.1 Initial Instrumented Tennis Racket

A custom instrumented tennis racket was designed to measure the forces and torques transferred to the wrist during game play. A commercial racket was purchased and a unidirectional surface mounted strain gauge was attached to it (Figure 3.1). The strain gage application procedure requires using GC-6 Isopropyl Alcohol to degrease the area of application, dry abrading the area with 220-grit silicon-carbide paper and then apply M-Prep Conditioner A to clean the surface. M-Prep Neutralizer 5A is then applied and scrubbed with a cotton-tipped applicator. Once the surface is appropriately cleaned and prepared, then the strain gage can be carefully attached to the surface. Micro-Measurement No. PCT-2A cellophane tape is needed to position the gage so that it is aligned with the marks previously drawn. After that, M-Bond 200 catalyst can be applied to the bonding surface of the gage and terminal to avoid the adhesive to harden. In this project, Micro-Measurement Certified M-Bond 200 adhesive was used because of its fast room-temperature cure and ease of application [39].

The strain gauge was connected to a commercial Data Acquisition system (cDAQ-9172, National Instruments Corporation, Austin, TX, United States) as seen in Figure 3.2 to measure the strain value obtained when a load was applied to the racket. The data sets performed using the DAQ system along with the results obtained are shown in the following subsections.

Figure 3.1: Strain gauge attached to the racket

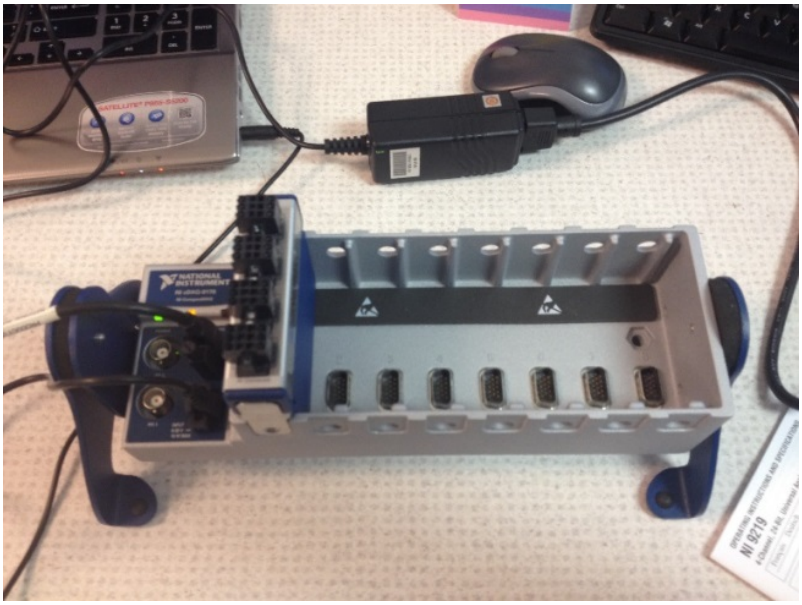

Figure 3.2: Data Acquisition System

3.1.1 Sensitivity Test of the Initial Design

Initial tests were performed to determine if the racket would be able to detect a tennis ball impact. A tennis ball was hit with the instrumented racket and the strain level recorded using the commercial DAQ (Figure 3.3). These results were compared with the tennis racket resting on the table under no load (Figure 3.4). The measured strain values for both conditions were very close to zero indicating that very little, if any, strain was measured during impact.

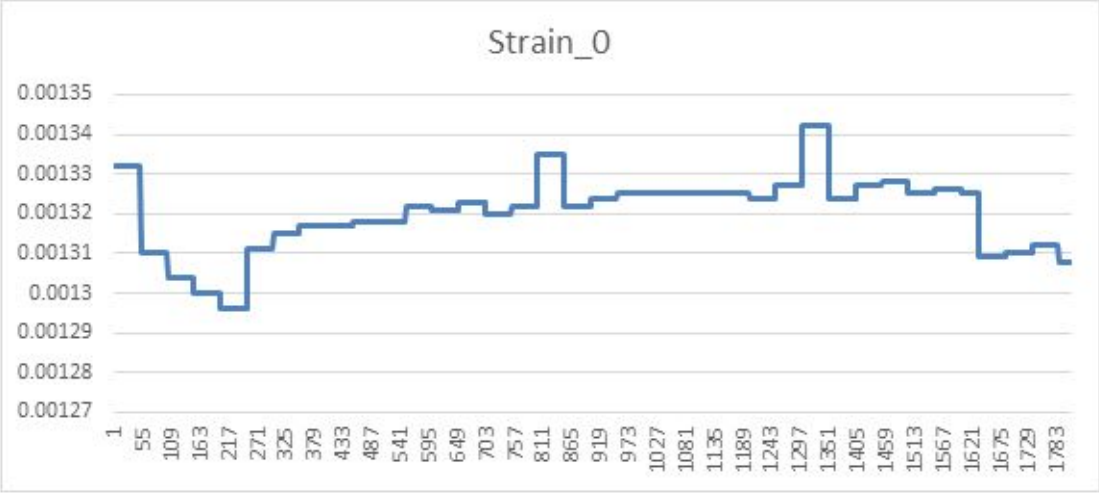

Figure 3.3: Strain level measured by the DAQ when hitting a tennis ball

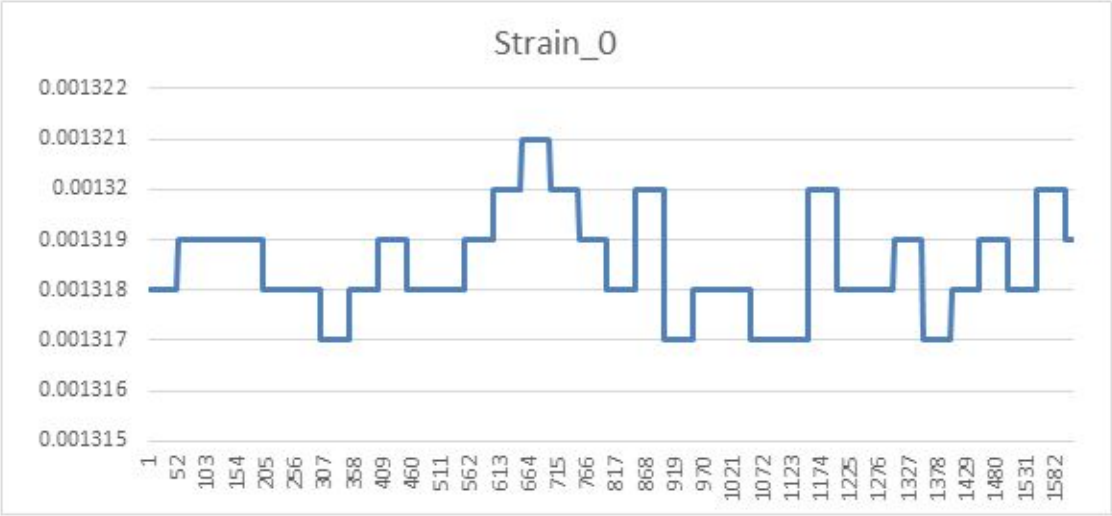

Figure 3.4: Strain level measured when racket is under no load

3.1.2 Evaluation of the Strain Gauge Configuration Using an Acrylic Beam

The lack of sensitivity in the previous test may be due to either a very low strain below the measureable threshold or problems configuring the DAQ. The operation of the DAQ was evaluated by attaching a strain gage to an acrylic beam clamped to the table that would attain considerably high strain when loaded (Figures 3.5 and 3.6).

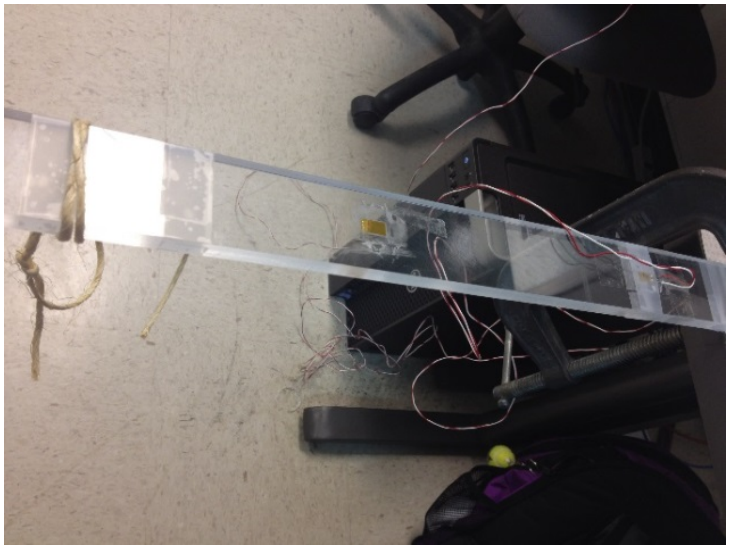

Figure 3.5: Experiment set-up using an acrylic beam

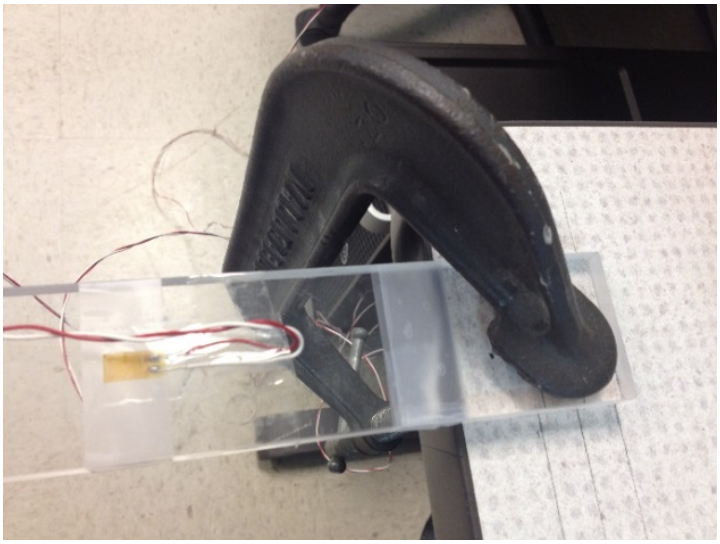

Figure 3.6: Acrylic beam clamped to the table

The plastic beam had a thickness of 1.8 cm, a length of 56 cm, and a width of 4.3 cm. It was clamped to the table with the strain gauge located 7.5 cm from the edge of the table. A 6.5 lbs weight was hung from the beam at a distance of 35 cm from the edge of the table and the voltage on the strain gage was measured. The weight was moved to 40 cm and the measurement repeated. The resistance between the strain gage and the load was calculated to be 27.5 cm or 35.5 cm, respectively. Strain was observed in the beam and measured during a static test and confirmed that the strain gauge and the DAQ were working. Therefore it was concluded that the original tennis racket was too stiff and producing strain levels below a measurable threshold.

Figure 3.7 shows the graph for the beam under no load. This signal corresponds to noise level with a magnitude of 4 uV.

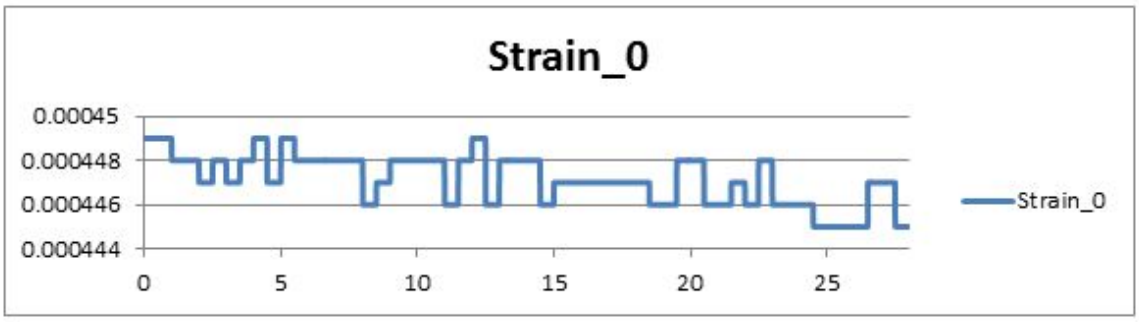

Figure 3.7: Acrylic beam under no load

Figure 3.8 shows the graph for the beam under no load for the first 10 seconds; then a constant and static load applied during the next 15 seconds, and no load applied during the last 10 seconds. By looking at the graph, the difference between load and no load can be easily seen. The load resulted in a change of voltage of approximately 2.25 mV resulting in a signal to noise ratio of 563:1.

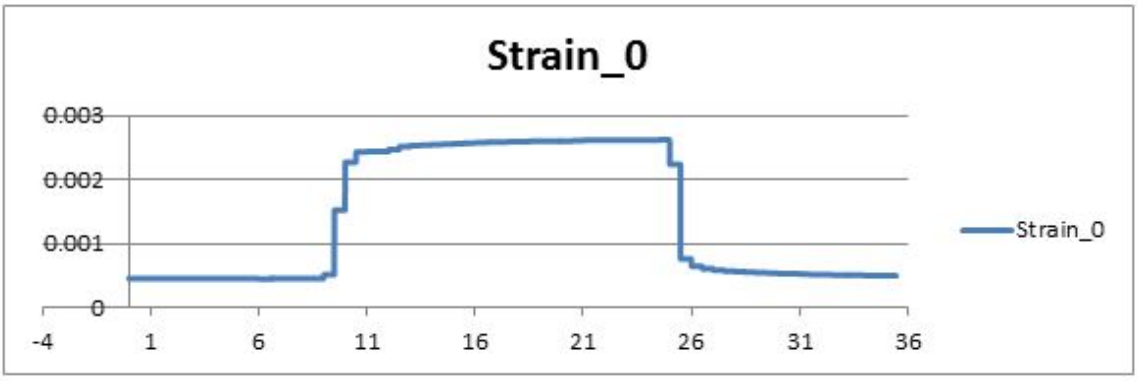

Figure 3.8: No load vs. load

3.1.3 Evaluation of Impact Response Using the Acrylic Beam

Given that strain was able to measure static loads, a new set of testing was performed to determine if the commercial DAQ would be able to detect a ball impact on the acrylic beam. Tests consisted on pushing and releasing the beam for longer times. All tests were taken at a sample rate of 100 Hz using 6.5 lbs load. Figure 3.9 shows random and quick push/release during 30 seconds. The waves appear to be square indicating a low speed data acquisition.

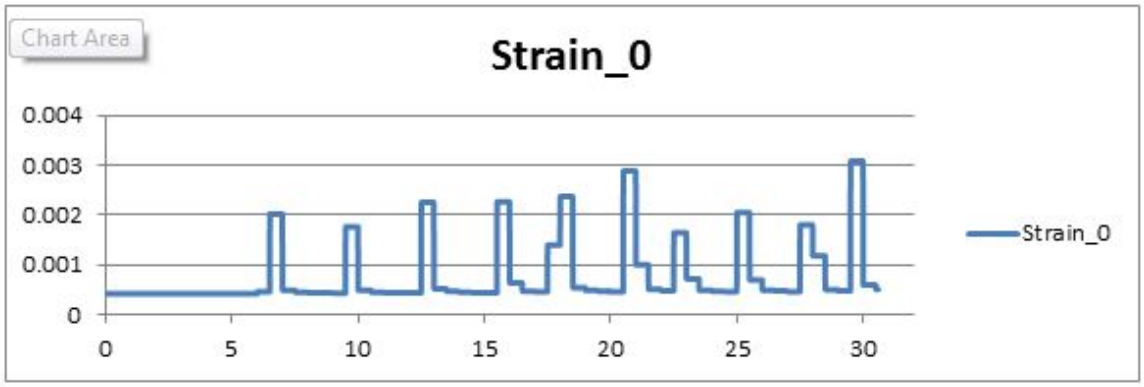

Figure 3.9: Quick push/release for 30 seconds

Several other tests were performed using the commercial DAQ system but the results were still unsatisfactory. The graphs obtained did not have enough data points throughout the signal. It was assumed that DAQ systems are most likely designed

for generally static loads, where the measured strain changes slowly over time. This differs from the impact of a tennis ball which requires a quick response from the system to be measured. Also, it is possible that a low pass filter is within the device that is used to attenuate high-frequency noise in the output.

3.2 Design of the Initial Quarter Wheatstone Bridge Circuit

The commercial DAQ system was found to be unable to detect the instant at which impact occurred, preventing any reliable measurements to be taken. To overcome this issue, a custom Wheatstone bridge circuit was designed. A DC Power Supply (E3631A, Agilent Technologies, Santa Clara, California) was used to provide 2.5 V to the circuit and an oscilloscope (54622D, Agilent Technologies, Santa Clara, California) was used to capture the waveform produced by the impact from start to end. An oscilloscope was selected because it was capable of very high speed (60 to 500 MHz) data acquisition. The first circuit was designed and built on breadboard (Figures 3.10 and 3.11), where R_1, R_2, R_3, and R_4 were fixed resistors, V_{OUT} is the output voltage, and V_{IN} is the input voltage. Resistors were measured because actual values varied from the theoretical. The resistances were measured to be 358 Ω, 357 Ω, 358 Ω and 356 Ω for R_1, R_2, R_3, and R_4, respectively.

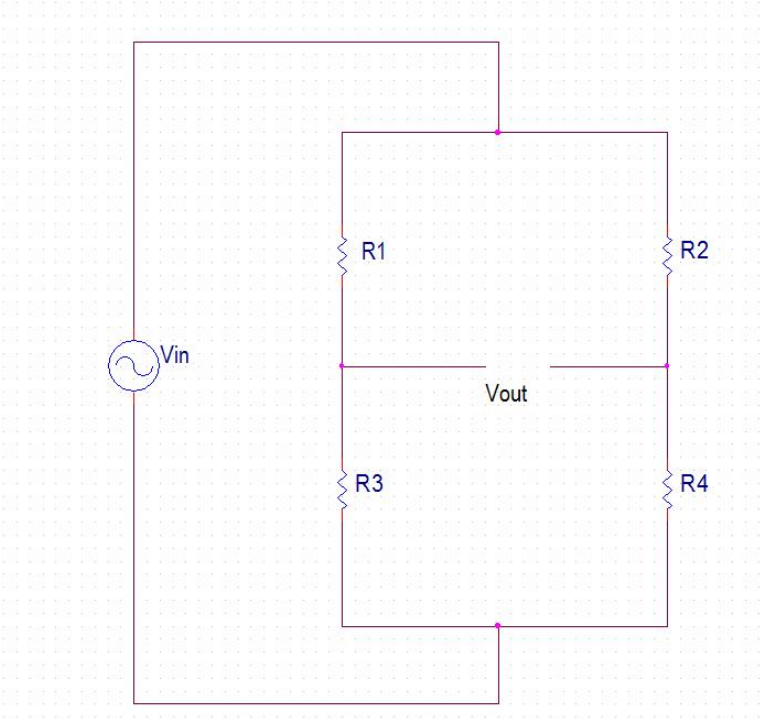

Figure 3.10: Schematic of first Wheatstone Bridge

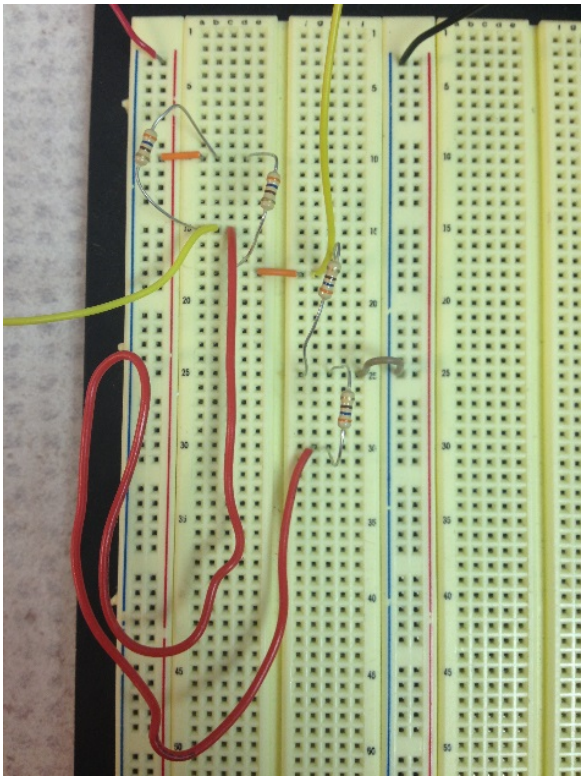

Figure 3.11: First Wheatstone Bridge on breadboard

The output voltage was measured for several input voltage and found to be non-zero. This indicated that the bridge was not balanced. To fix these problems, a potentiometer (variable resistor) was introduced to replace R_4 while the rest of the configuration remained the same as shown in Figure 3.12. The potentiometer was adjusted voltage out was reduced to 0.001 mV to 0.079 mV. This is a much better output than the one obtained using four fixed resistors. However, a value of zero volts across the bridge could not be achieved.

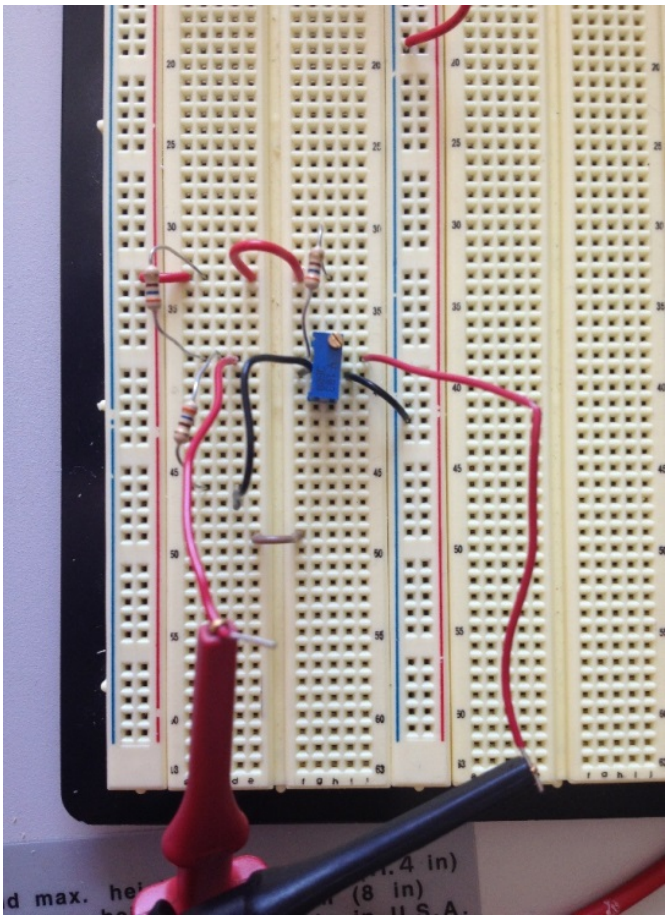

Figure 3.12: Wheatstone Bridge circuit using a potentiometer

3.3 Improved Instrumented Tennis Racket with Final Electrical Custom Circuit

Since stiffness of the racket was found to be tool high, it was concluded that a new instrumented tennis racket was needed with stiffness below that of a regular racket. A new commercial racket was purchased and customized for the purpose of the experiment as seen in Figure 3.4. The regular handle was cut out and substituted with a 2.54 cm diameter acetyl rod to reduce the level of stiffness of the regular racket. The new handle was notched using a Haas VF-1 4 axis mill and was attached to the frame of the racket by two 20 gauge mild steel pieces (one on each side) previously cut using a 500W CO2 Haas laser cutter. The pieces of steel were secured by bolts. The material used to build the new instrumented tennis racket added additional weight to the racket, increasing it from 320 g to 680 g. Once the new instrumented was built (Figure 3.13), unidirectional as well as triaxial strain gauges were attached to the handle of the racket using the methods previously described.

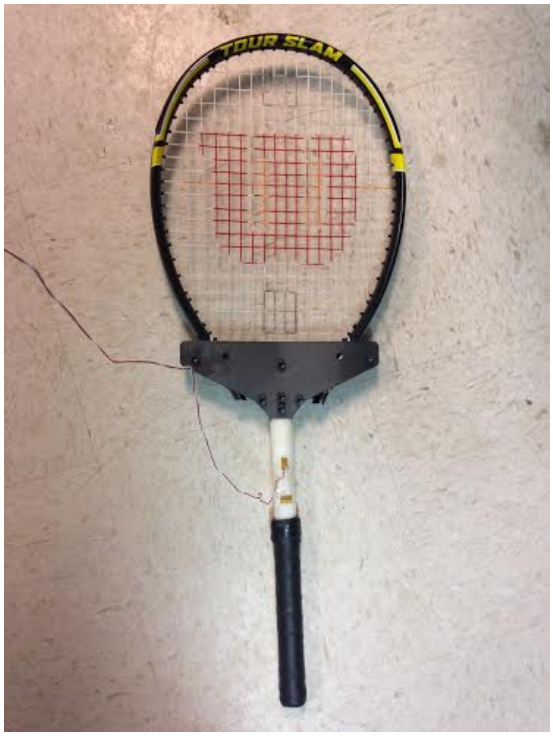

Figure 3.13: New instrumented tennis racket

Based on the circuit configuration in Figure 3.10, a new circuit was designed and built. Figure 3.14 shows the schematic of the new analog circuit where resistors $R_{11} = R_{22} = R_{33} = 357\ \Omega$(actual values vary from theoretical) and the strain gauge was placed on the fourth arm of the Wheatstone Bridge. The output voltage of the Wheatstone Bridge was amplified by the LMC6484 operational amplifier, where $R_1 = R_3 = 1\ M\Omega$, and $R_2 = R_4 = 100\ K\Omega$ (actual values vary from theoretical). Therefore, the voltage gain of the operational amplifier was calculated to be

$$A_v = \frac{R_1}{R_2} = \frac{1\ M\Omega}{100\ K\Omega} = 10 \tag{3.1}$$

To amplify the signal out of the sensor circuit (Vout1), a non-inverting amplifier was added, where the source resistor $R_S = 10\ K\Omega$, and the feedback resistor $R_F = 150\ K\Omega$. The new operational amplifier was added to increase the voltage level to a range that was easily readable by the oscilloscope. In this case, the voltage gain was calculated to be

$$A_v = \frac{V_{out2}}{V_{out1}} = 1 + \frac{R_F}{R_S} = \frac{150\ K\Omega}{10\ K\Omega} = 16 \tag{3.2}$$

As a result, Vout2 was 16 times greater than Vout1.

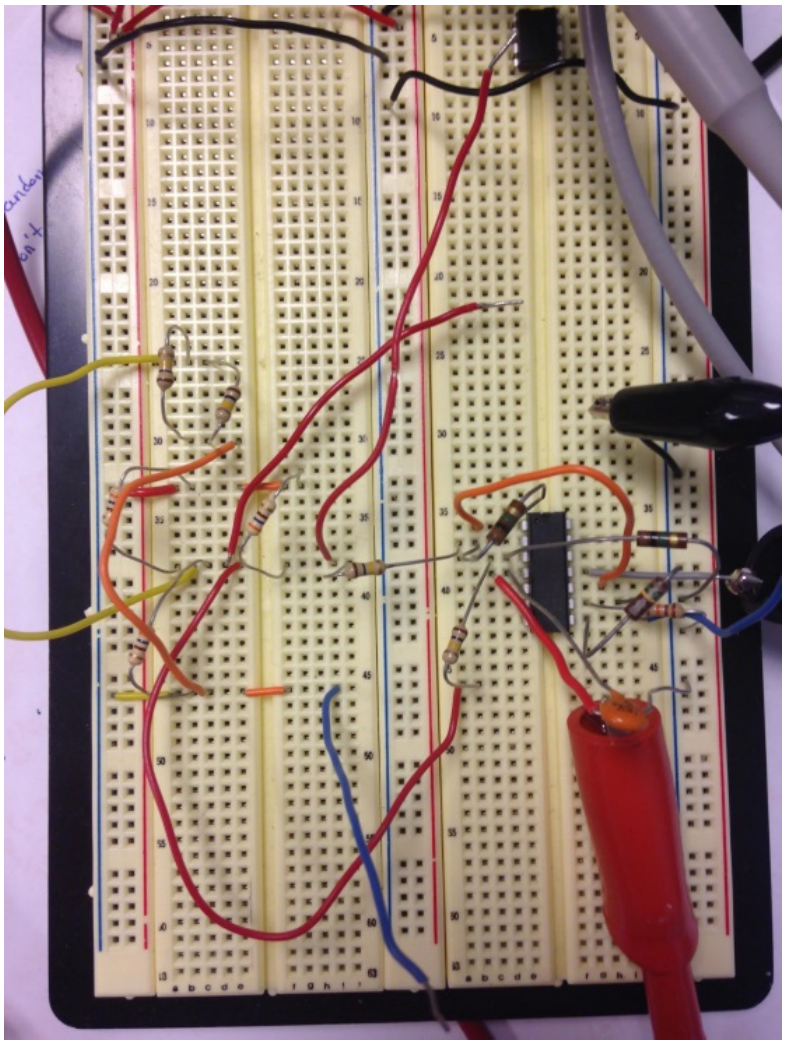

Figure 3.14: Custom electrical circuit built on breadboard

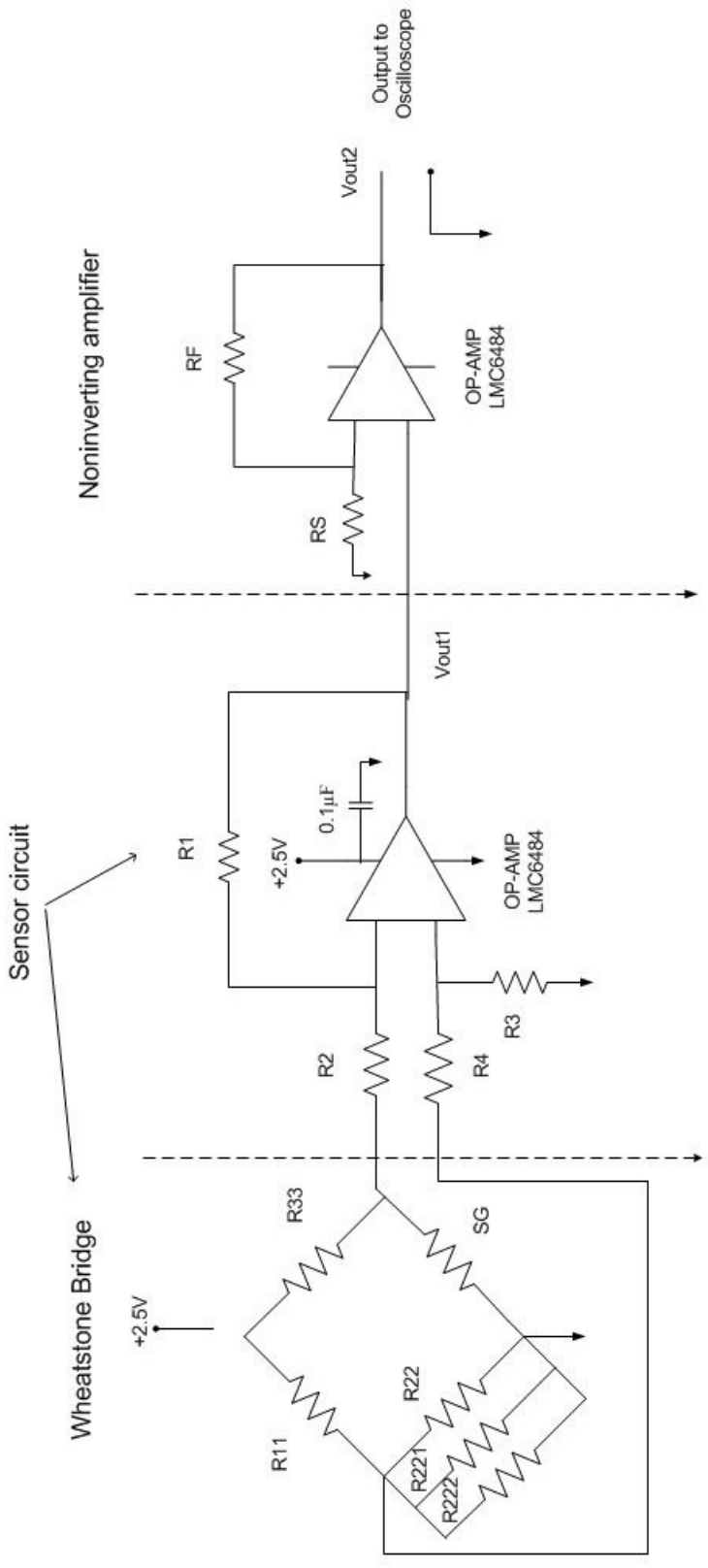

Figure 3.15: Schematic of custom electrical circuit

When the strain gauge resistance changes due to the impact between the tennis racket and the ball, the signal will pass through the sensor circuit (Figure 3.16). This signal will be amplified by the operational amplifiers and the voltage output will be shown on the oscilloscope. This data is then transferred to the computer.

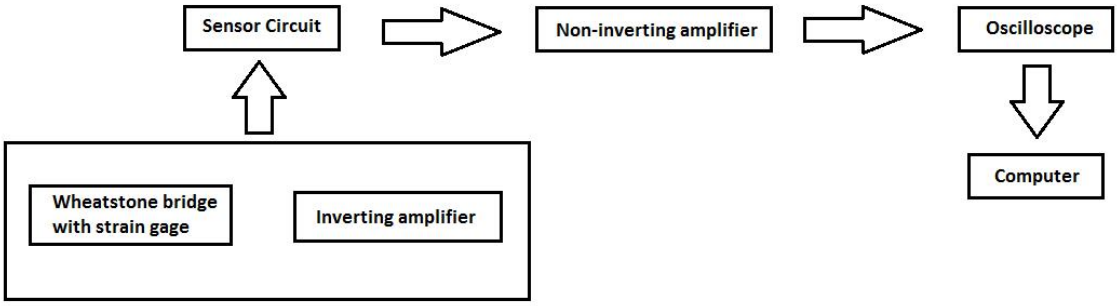

Figure 3.16: Block diagram of the overall process

A soldered prototype board was built to avoid misconnections that could occur during the testing session if a breadboard design was used. The circuit described in Figure 3.14 was built four times in order to provide enough channels for the uniaxial and triaxial strain gages. The prototype board can be seen in the following figures.

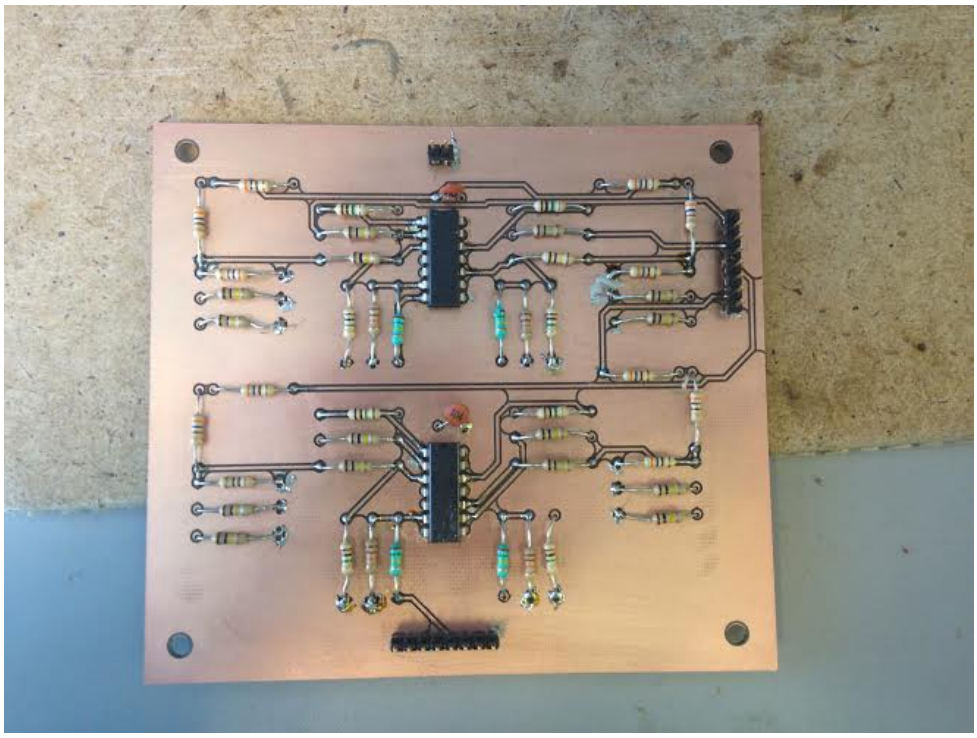

Figure 3.17: Top part of the prototype board

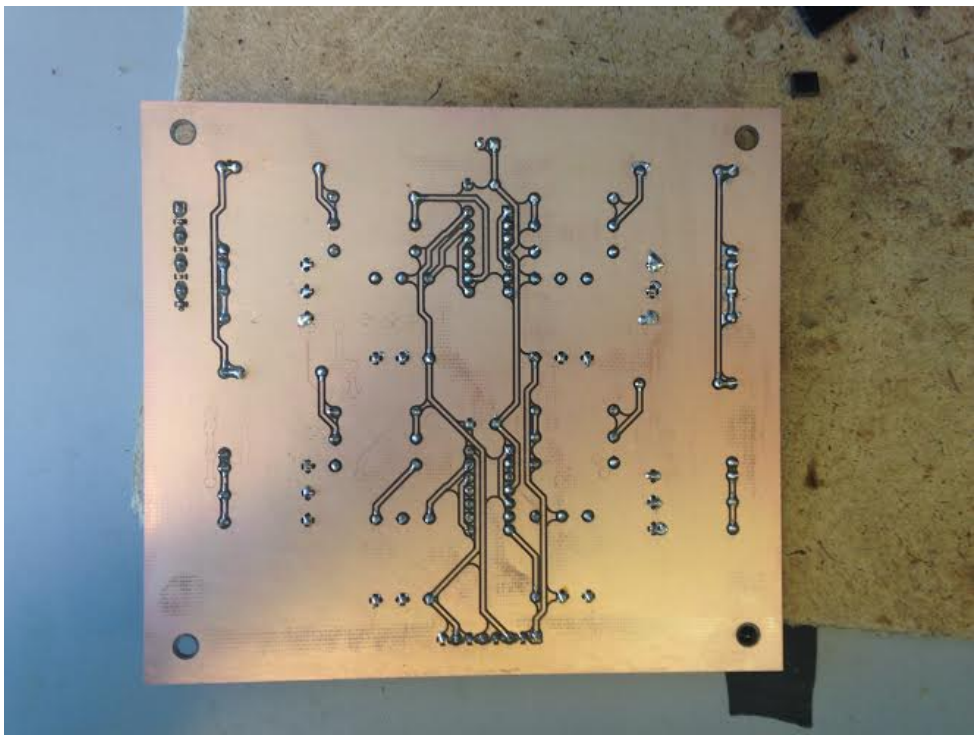

Figure 3.18: Bottom part of the prototype board

3.4 Tennis Racket Calibration

Three different calibration tests were performed to determine the relationship between externally applied loads and the strain within the racket shaft caused by the bending moment. The procedure was the same for each test. The racket was clamped to the table and four different spots were picked on the tennis racket (edge of the beam, bottom-point, mid-point and top-point) as seen in Figure 3.19. First, the voltage when no load was applied was taken to serves as a reference for the rest of the measurements. Then a load was applied (one at a time) at each of the points and the resulting voltages were measured on the oscilloscope. The load for each calibration test was different.

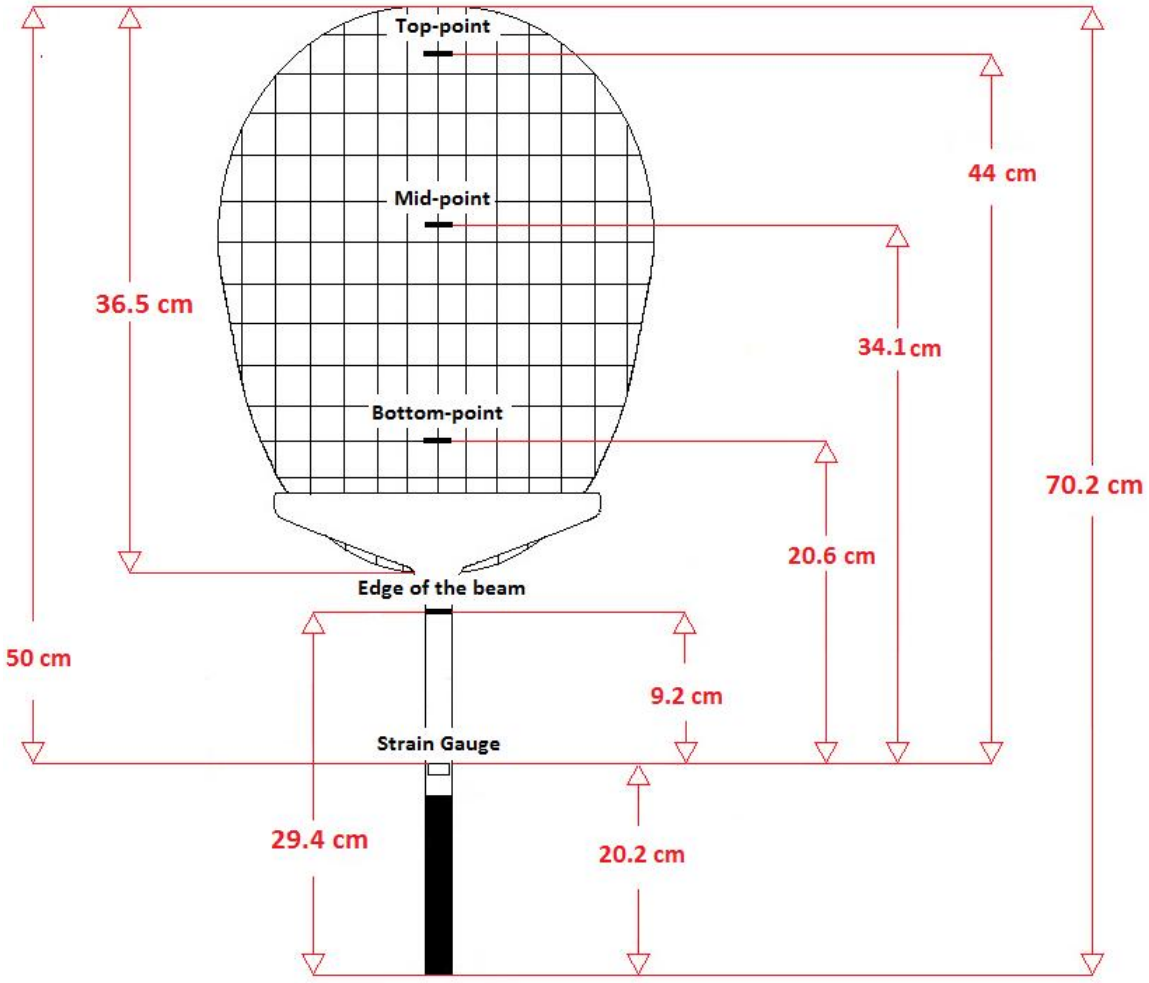

Figure 3.19: Racket diagram with distances used for calibration measurements

Calibration 1 was performed using a load of 3 kg. The voltages obtained for each of the measurements were subtracted from the voltages obtained when no load was applied (1.47 V) to find the scaled voltages as seen in Table 3.1.

Table 3.1: Data corresponding to calibration 1

	Distance from load to strain gage (cm)	Voltage obtained from oscilloscope (V)	Scaled voltage (V)
No load	N/A	1.47	0
Load edge beam	9.2	1.39	0.08
Load bottom-point	20.6	1.16	0.31
Load mid-point	34.1	0.911	0.559
Load top-point	44	0.746	0.724

Figure 3.20 shows the voltage as a function of distance corresponding to Calibration 1. A trendline was used to show the linear relationship between the two variables (distance and voltage). It can be seen that the voltage increases as the distance increases.

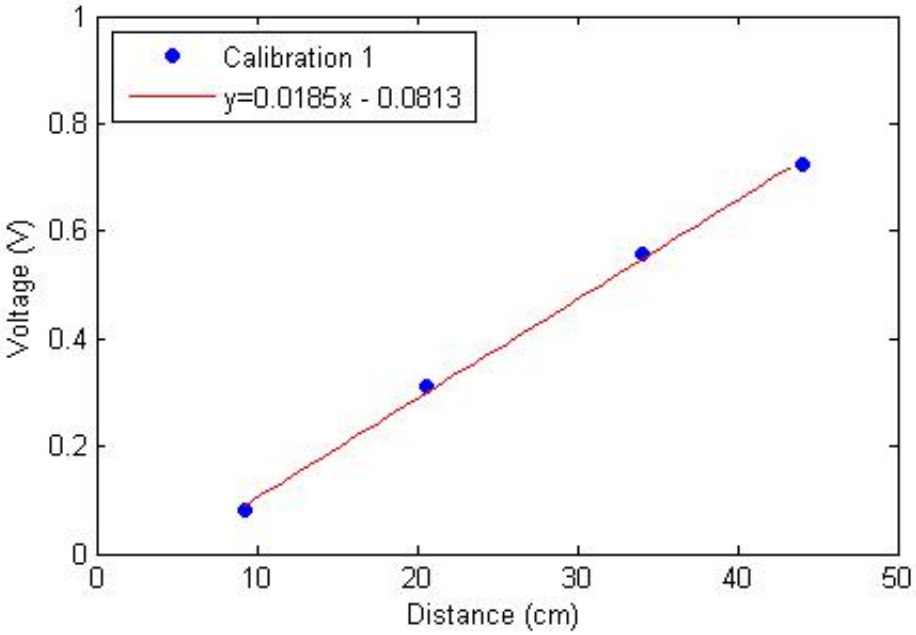

Figure 3.20: Calibration 1 scaled voltages as a function of distance

Calibrations 2 and 3 were performed following the same procedure as Calibration 1. The loads were equal to 1.773 kg and 1.182 kg, respectively. Data corresponding to Calibrations 2 and 3 can be seen in Table 2.

Table 3.2: Data corresponding to calibrations 2 and 3

		Calibration 2		Calibration 3	
Load	Distance from load to SG	Voltage from Oscilloscope (V)	Scaled Voltage (V)	Voltage from Oscilloscope (V)	Scaled Voltage (V)
None	N/A	1.37	0	1.37	0
Edge beam	9.2	1.33	0.04	1.32	0.05
Bottom-point	20.6	1.15	0.22	1.23	0.14
Mid-point	34.1	0.994	0.376	1.11	0.26
Top-point	44	0.874	0.796	1.04	0.33

Figure 3.21 shows the voltage as a function of distance corresponding to Calibrations one through three. Trendlines are used to show the linear relationship between the two variables (distance and voltage). As it can be seen, the voltage increases as the distance increases in all three calibrations. Although three different calibrations were performed and the average of them could have been used, it was decided to use Calibration 1. It was selected because the voltages measured during impact were higher and Calibration 1 had values closer to this number.

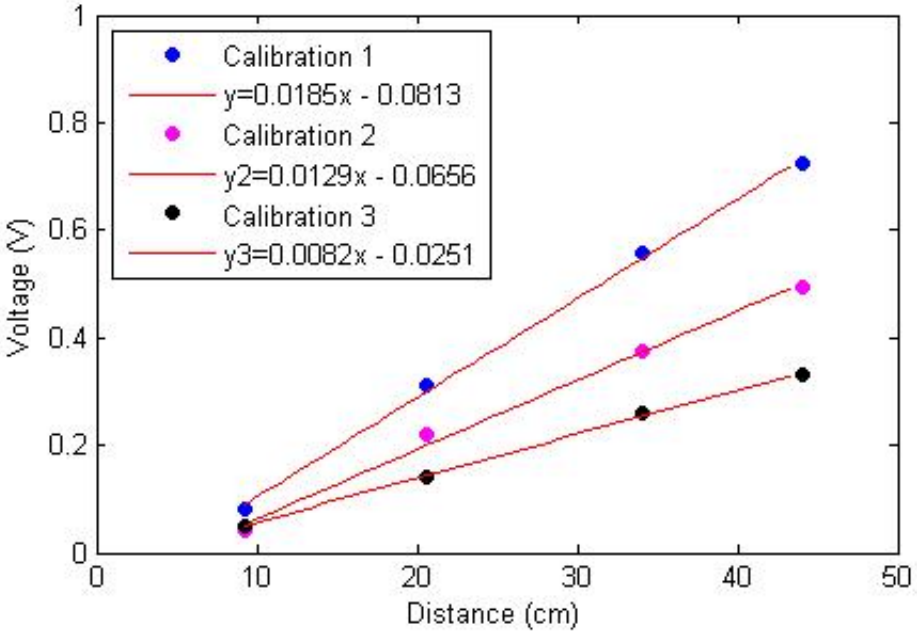

Figure 3.21: Scaled voltages as a function of distance for the calibration measurements

3.5 Collection of Impact Data During Game Play

Two participants were recruited for the study, one male recreational player and one female athlete tennis player. This was done so that the data would be more consistent because the same person will be hitting the ball multiple times. The participants completed a demographic data sheet and signed an informed consent form approved by the institutional review board (IRB) at Western Carolina University prior to participating in the study. Participants were provided with the instrumented racket and were asked to stand behind the service line. The test consisted of hitting a total of twenty regular serves split into 4 different sets of 5 serves each. The overall test for the male participant took about 1 hour and the female participant took about 30 minutes. The difference in time was due to some difficulties encountered in the process of transferring the data from the oscilloscope to the computer using a custom Labview 2012 program called ScopeGrab. Participants were photographed during the

serve using a GoPro Hero3 (GoPro, Inc, San Mateo, California, United States) high speed camera (Figure 3.22) at 120 frames per second. These photographs would later be used to identify the ball impact location of each serve.

Figure 3.22: GoPro Hero3 high speed video camera

Figure 3.23 shows the overall scene of the set up for the testing. The high speed video camera was placed at approximately 45 angle from the male recreational player performing the test using the baseline as the reference (horizontal axis). Figure 3.24 shows the custom electrical circuit connected to the DC power supply and to the oscilloscope. The oscilloscope was connected to the computer to store the data.

Figure 3.23: Recreational tennis player hitting a tennis serve during testing

Figure 3.24: Set-up for testing at the tennis courts

CHAPTER 4: ANALYSIS AND RESULTS

4.1 Analysis of Photographic Data

The recorded videos of each overhead hit were opened with the MAGIX Movie Edit Pro 2014 Plus (MAGIX Computer Products International Corporation, Reno, NV, United States). Using the editor, each hit was analyzed frame by frame to identify the frame where the ball made contact with the racket. A screenshot of each impact was taken. A total of forty images were printed and the distances from the center of the ball (CB) to the strain gauge (SG) and the distance from the strain gauge to the top of the racket (TR) were measured. The measured distances in the photographs were then compared to the actual distances on the instrumented racket and the ratio of distances was used to determine the actual distance between the center of the ball and the strain gauge as well as the distance from the center of ball to the center of the hand as seen in equation below.

$$\frac{measured\ x_{TR-SG}}{actual\ x_{TR-SG}} = \frac{measured\ x_{CB-SG}}{actual\ x_{CB-SG}} \tag{4.1}$$

Where x_{TR-SG} is the distance from the top of the racket to the strain gauge, and x_{CB-SG} is the distance from the center of the ball to the strain gauge.

Athlete tennis player serve number 10 (Figure 4.2) was considered typical and the detailed calculation methods used to analyze the data are shown below. First, the distance from the center of the ball to the strain gauge was calculated.

$$\frac{14.6\ cm}{50\ cm} = \frac{9.2\ cm}{actual\ x_{CB-SG}} \tag{4.2}$$

Where

$$actual\ x_{CB-SG} = 31.51\ cm \tag{4.3}$$

The distance from the center of the ball to the center of the hand was calculated by adding 13.2 cm (distance between strain gauge and center of the hand) to the actual distance from the center of the ball to the strain gauge.

$$actual\ x_{CB-CH} = 31.51\ cm + 13.2\ cm \tag{4.4}$$

$$= 44.71\ cm \tag{4.5}$$

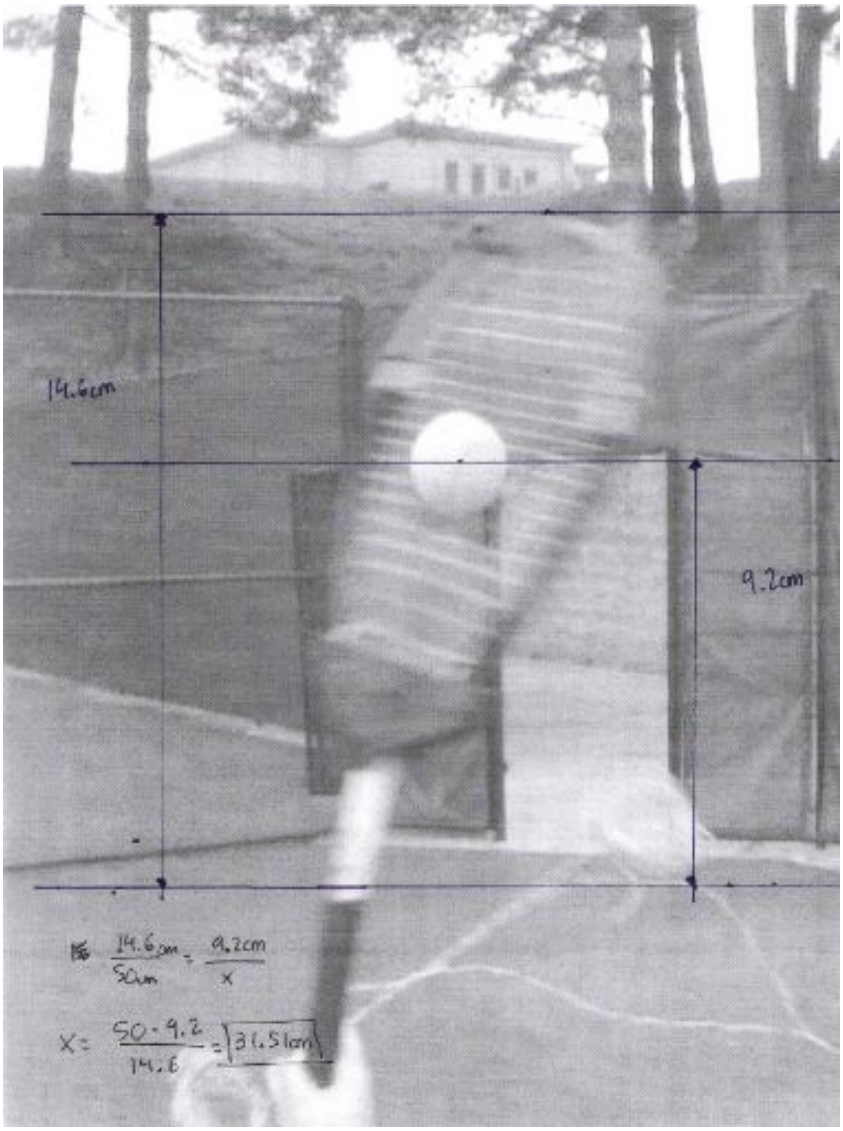

Figure 4.1: Printed image with measured distances

The same process was used to calculate all the corresponding distances for each serve for both participants.

4.2 Analysis of Strain Data

The data obtained from the oscilloscope was exported into MS Excel (Microsoft Corp, Redmond, Washington, United States) to obtain the x and y coordinates of each data point. These data points were imported into Matlab (The MathWorks, Natick, Massachusetts, United States) to create two .mat files. 'Female Serve Data From Oscilloscope.mat' contains the x and y coordinates for the twenty serves performed by the female participant. 'Male Serve Data From Oscilloscope.mat' contains the x and y coordinates for the twenty serves performed by the male participant. These files were loaded into 'Female Graphs From scilloscope.m' and 'Male Graphs From Oscilloscope.m' (custom matlab code) respectively, and a plot was created for each serve.

Figure 4.2 corresponds to the graph of the athelte tennis player's serve number 10 over a period of one second. The signal remained constant at a voltage level of 1.42 V when the racket was at rest. The period of time from approximately -0.2 s to 0.05 s corresponds to the backswing of the racket. The backswing will have a negative or positive deflection depending on the orientation of the strain gauge when impacting the ball. If the strain gauge is facing the net when the racket hits the ball, then the backswing will have a negative deflection; positive deflection will occur if the strain gauge is facing the opposite direction. The acceleration phase or forward swing takes place between 0.05-0.128 s which is the short period of time in which the participant brings the racket up and forward prior to impact. Backward and forward strokes will always have opposite deflections on the graph. Therefore, depending on the orientation of the racket, at impact the signal will either go up or down. The impact occurs at 0.128 s which causes the oscillations in the signal. Figure 4.3 shows

a closer look of the oscillations during and after impact of a regular serve.

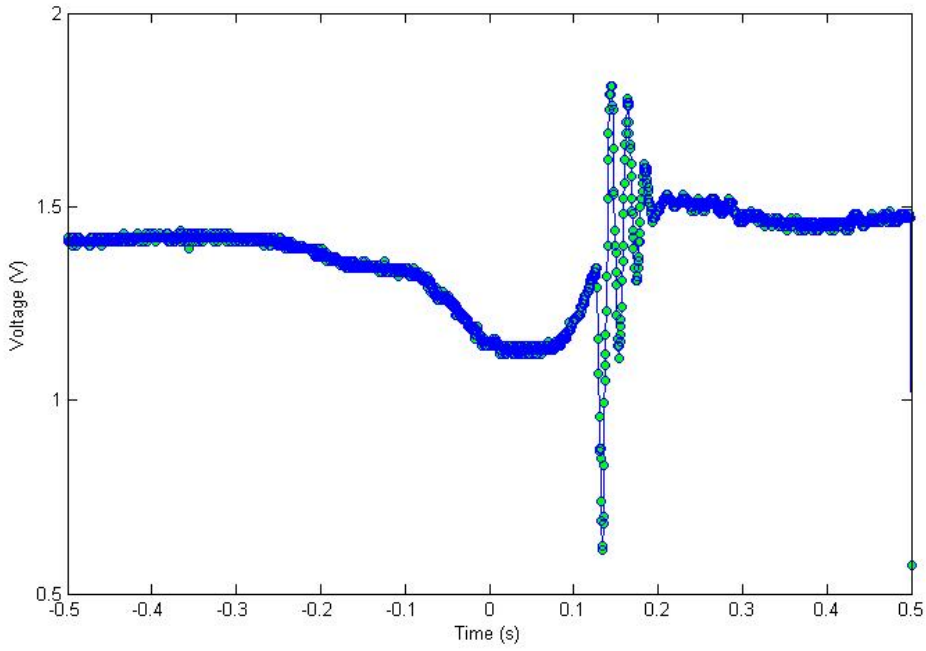

Figure 4.2: Graph corresponding to athlete tennis player's serve 10

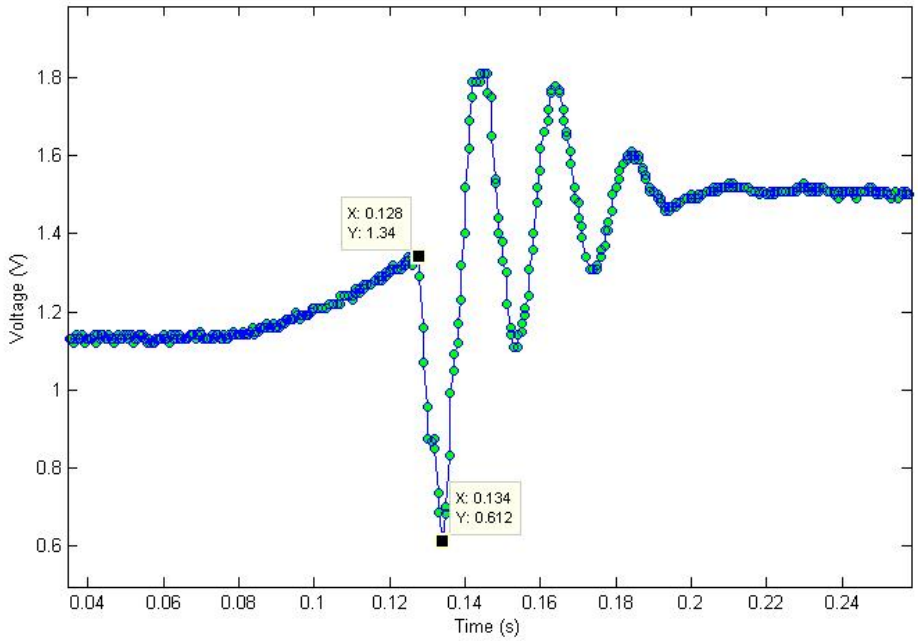

Figure 4.3: Close up of Figure 4.2

Voltage difference between no load voltage (when racket was at rest) and highest/lowest peak value (depending on the orientation of the strain gauge when impact occurred) was obtained

$$V_{diff} = V_{noload} - V_{peak} \tag{4.6}$$

$$= 1.42\ V - 0.612\ V \tag{4.7}$$

$$= 0.808\ V \tag{4.8}$$

4.3 Calculations of Forces and Moments

Forces and bending moments were calculated for both participants. Athlete tennis player's serve number 10 (Figure 4.2) was selected to show a thorough description of the calculations. Using the equation relating voltage to distance from Calibration 1, and the distance from the strain gauge to the center of the ball, the voltage that a 3kg load would produce as this distance was calculated

$$y = 0.0185x_{CB-SG} - 0.0813 \tag{4.9}$$

$$= 0.0185(34.51\ cm) - 0.0813 \tag{4.10}$$

$$= 0.594135\ V \tag{4.11}$$

where y is the voltage according to graph obtained from Calibration 1, and x_{CB-SG} is the distance from the center of the ball to the strain gauge.

A ratio between loads and voltages was used to calculate the corresponding load for the voltage at impact,

$$\frac{3\ Kg}{0.594135\ V} = \frac{x_{load}}{0.808\ V} \tag{4.12}$$

$$x_{load} = \frac{3\ kg * 0.808\ V}{.594135\ V} x_{load} = 4.07988\ kg \tag{4.13}$$

where x_{load} is the equivalent value of a free hanging mass that would result in the same voltage if hung at the ball impact distance

The force value was calculated using Newtons Second Law,

$$F = ma \tag{4.14}$$

$$= (4.07988\ Kg)(9.81\ \frac{m}{s^2}) \tag{4.15}$$

$$= 40.0236\ N \tag{4.16}$$

where F is the force, m is the mass, and a is the acceleration.

Using the peak force at the ball impact location, the bending moment at the hand was calculated,

$$m_{CH} = F * x_{CB-CH} \tag{4.17}$$

$$= (40.0236\ N) * (0.4471\ m) \tag{4.18}$$

$$= 19.8957\ Nm \tag{4.19}$$

where m_{CH} is the bend bending moment at the hand. F is the force an x_{CB-CH} is the distance from the center of the ball to the center of the hand.

Tables 3 and 4 show the values obtained for the serves performed by both the athlete and the recreational tennis players.

Table 4.1: Athlete tennis player's calculations

Serve #	Distance from CB to SG (cm)	Distance from CB to CH (cm)	v_{diff} (V)	Calibration 1 y=0.0185x 0.0813	Mass (kg)	Peak Force (N)	Bending Moment at hand (Nm)
1	39.96	53.16	0.658	3	0.65796	29.43	15.6459
2	38.73	51.93	0.827	3.9058	0.6352	38.3161	19.8976
3	40.91	54.11	0.77	3.4195	0.6755	33.5454	18.1514
4	39.54	52.74	0.852	3.9312	0.6502	38.5647	20.339
5	33.05	46.25	0.67	3.7916	0.5301	37.1952	17.2028
6	35	48.2	0.483	2.5592	0.5662	25.1054	12.1008
7	45	58.2	0.902	3.6022	0.7512	35.3379	20.5667
8	37.03	50.23	0.714	3.5478	0.6038	34.8039	17.4819
9	38.21	51.41	0.739	3.5439	0.6256	34.7655	17.8729
10	36.51	49.71	0.808	4.0799	0.5941	40.0236	19.8958
11	38.11	51.31	0.77	3.7035	0.62.7	36.3313	18.6416
12	40.12	53.32	0.902	4.0943	0.6609	40.1650	21.4159
13	34.48	47.68	0.427	2.3016	0.5566	22.5783	10.7353
14	35.16	48.36	0.714	3.7634	0.5695	36.9194	17.8542
15	32.19	45.39	0.452	2.6370	0.5142	25.8693	11.7421
16	41.31	54.51	0.902	3.9623	0.6829	38.8703	21.1882
17	40.57	53.77	0.902	4.0434	0.6692	39.6654	21.3281
18	40.85	54.05	0.895	3.9812	0.6744	39.0553	21.1094
19	39.39	52.59	0.764	3.5402	0.6474	34.7297	18.2643
20	33.753	46.95	0.427	2.3588	0.5431	23.1397	10.8641

Table 4.2: Recreational tennis player's calculations

Serve #	Distance from CB to SG (cm)	Distance from CB to CH (cm)	v_{diff} (V)	Calibration 1 y=0.0185x 0.0813	Mass (kg)	Peak Force (N)	Bending Moment at hand (Nm)
3	29.11	42.31	0.16	1.0498	0.4572	10.2984	4.3573
4	26.88	40.08	0.14	1.0097	0.4159	9.9048	3.9698
5	33.72	46.92	0.37	2.0460	0.5425	20.0713	9.4175
6	40.36	53.56	0.79	3.5619	0.6654	34.9430	18.7155
7	35.82	49.02	0.52	2.6833	0.5814	26.3233	12.9037
8	24.49	37.69	0.24	1.9367	0.3718	18.9991	7.1608
9	40.94	54.14	0.78	3.4612	0.6761	33.9532	18.3823
10	37.72	50.92	0.69	3.3576	0.6165	32.9376	16.7718
11	46.91	60.11	0.69	2.6318	0.7865	25.8179	15.5192
12	39.75	52.95	0.59	2.7061	0.6541	26.5469	14.0566
13	34.41	47.61	0.35	1.8909	0.5553	18.5499	8.8316
14	39.47	52.67	0.62	2.8664	0.6489	28.1195	14.8105
15	35.92	42.12	0.45	2.3147	0.5832	22.7076	11.1539
16	43.94	57.14	0.69	2.8295	0.7316	27.7569	15.8603
17	36.74	49.94	0.57	2.8577	0.5984	28.0337	14
18	41.51	54.71	0.61	2.6652	0.6866	26.1453	14.3041
19	41.57	54.77	0.65	2.8354	0.6877	27.8148	15.2342
20	38.33	51.53	0.69	3.2972	0.6278	32.3456	16.6677

Although serves number 1 and 2 from recreational tennis player were hit properly as seen in Figures 4.4 and 4.5, the waveforms collected with the oscilloscope were unusual (compare Figures 4.7 and 4.8 to the Figure 4.6). Signal corresponding to serve 1 was not obtained due to an early or late stop of the signal on the oscilloscope and the time where impact occurred was missed. The signal corresponding to serve 2 (Figure 4.8) resulted in an atypical waveform. This may have been caused by a slight loss of power for a brief period of time making the oscillation unable to properly capture the signal. As a result, both serves 1 and 2 were removed from the experimental data set.

Figure 4.4: Recreational tennis player ball impact corresponding to serve 1

Figure 4.5: Recreational tennis player ball impact corresponding to serve 2

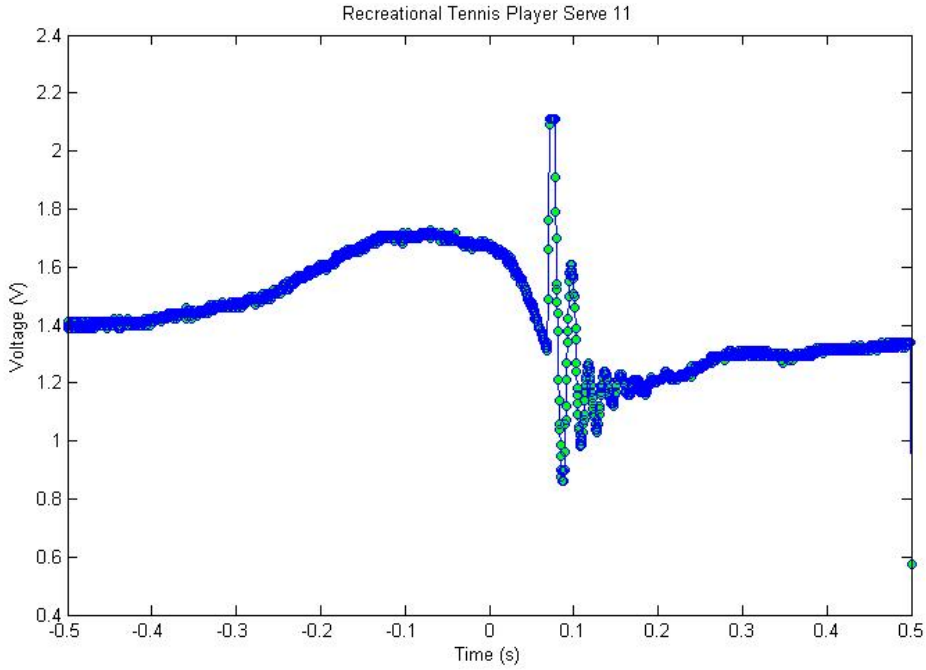

Figure 4.6: Recreational tennis player graph of ball impact corresponding to serve 11

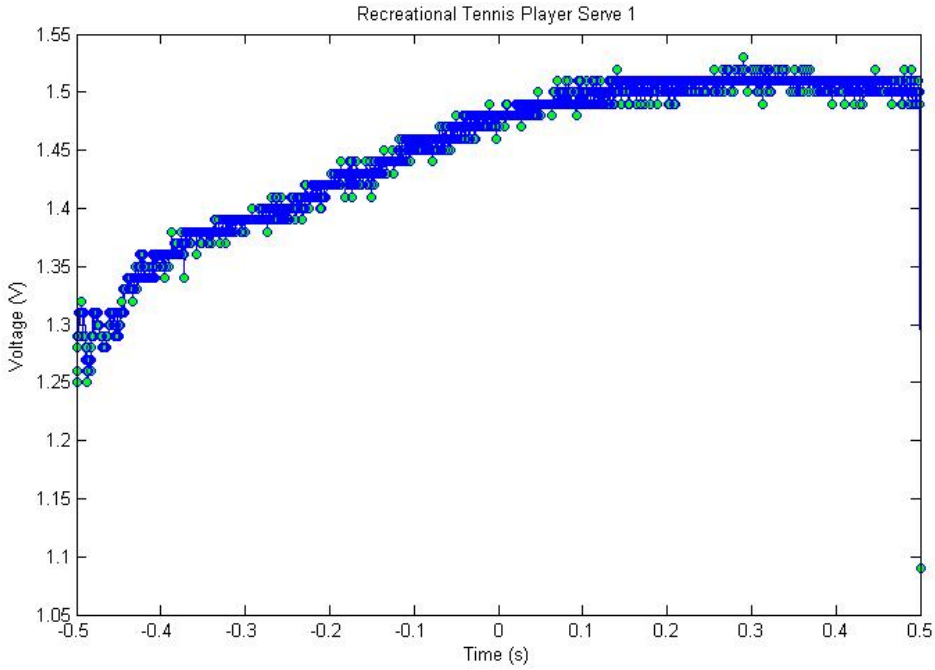

Figure 4.7: Recreational tennis player graph of ball impact corresponding to serve 1

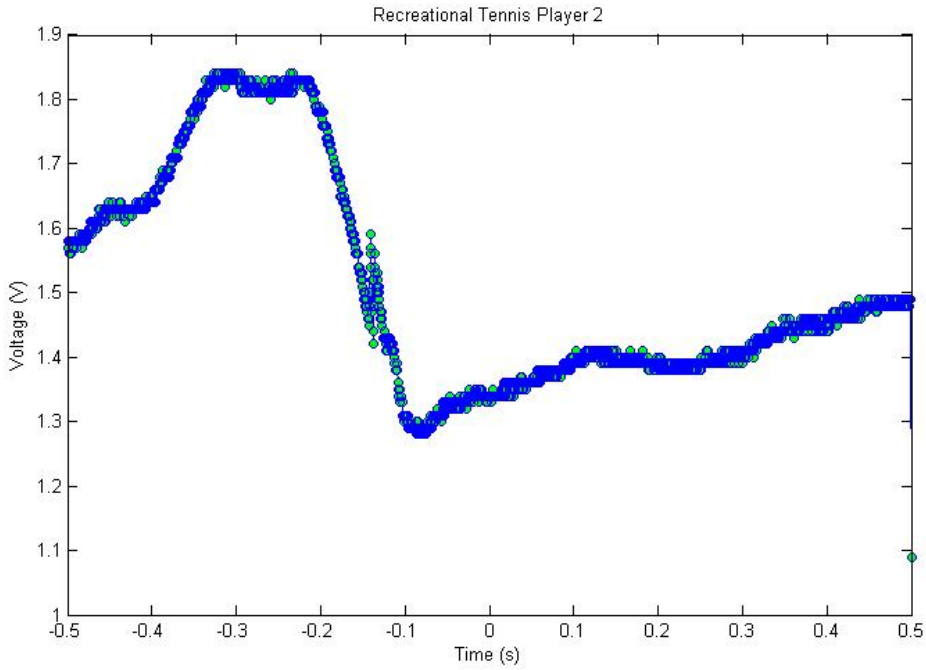

Figure 4.8: Recreational tennis player graph of ball impact corresponding to serve 2

4.4 Calculations of Velocities

A linear relationship exists between the change in linear momentum and the impulse,

$$Imp = \int_{t_0}^{t_1} F dt = \delta m = m(v_f - v_i) \tag{4.20}$$

where Imp is the impulse, F is the force, δm is the change in linear momentum, m is the mass of the ball, v_f is the ball velocity after impact and v_i is the initial ball velocity. By determining the impulse, the velocity can be calculated.

The Riemann sum was used to approximate the integral of the voltage over the period of time in which the racket and the ball were in contact. Error needs to

be taken into account since velocities were approximated based on previous values.

$$A = \int_{0.128}^{0.14} V dt \tag{4.21}$$

$$= 0.0045875\ Vs \tag{4.22}$$

This value was used to calculate the impulse over that period of time which corresponds to the change in momentum over that time as seen on equation 4.20.

The ratio between loads and voltages (equation 4.13) was used to calculate the corresponding load for that period of time

$$x_{load} = \frac{3\ kg * 0.0045875\ V}{.594135\ V} x_{load} = 0.02310938\ kg \tag{4.23}$$

The impulse of the impact was calculated as follows

$$Imp = F = ma \tag{4.24}$$

$$= (0.02310938\ Kg)(9.81\ \frac{m}{s^2}) \tag{4.25}$$

$$= 0.2267024074\ Ns \tag{4.26}$$

Given the ball has a mass of 57g and assuming a zero initial horizontal velocity, the velocity of the ball after impact can be calculated by using the second equality of equation 4.20

$$Imp = mv_f \tag{4.27}$$

$$v_f = \frac{0.2267024074\ Ns}{0.057\ kg} \tag{4.28}$$

$$= 3.9772352175\ \frac{m}{s} = 14.31804678\ \frac{km}{h} \tag{4.29}$$

These results for the impulse and velocities do not account for momentum transfer between the racket and the ball. They are approximations based on the strain voltages and forces previously obtained. Thus actual ball velocities will be much higher than the ones shown in Tables 5 and 6.

Table 4.3: Athlete tennis player's ball velocity calculations

Serve #	Ball velocity after impact ($\frac{km}{h}$)
1	17.74
2	18.68
3	16.08
4	13.74
5	19.65
6	10.30
7	16.71
8	14.81
9	12.44
10	14.35
11	15.90
12	17.87
13	7.72
14	13.77
15	7.29
16	18.97
17	18.89
18	19.10
19	16.84
20	9.17

Table 4.4: Recreational tennis player's ball velocity calculations

Serve #	Ball velocity after impact ($\frac{km}{h}$)
3	3.84
4	2.79
5	8.55
6	15.36
7	12.40
8	12.02
9	16.92
10	16.06
11	16.84
12	13.34
13	10.51
14	14.90
15	9.85
16	16.61
17	13.49
18	15.22
19	14.13
20	16.59

4.5 Results of Forces and Moments

Before plotting the forces and moments previously obtained, a boxplot was run for each participants to eliminate the possibility of having outliers (points that are further away from the mean than what is deemed reasonable) within the data. No outliers were found in either data set as it can be seen in Figures 4.9 and 4.10.

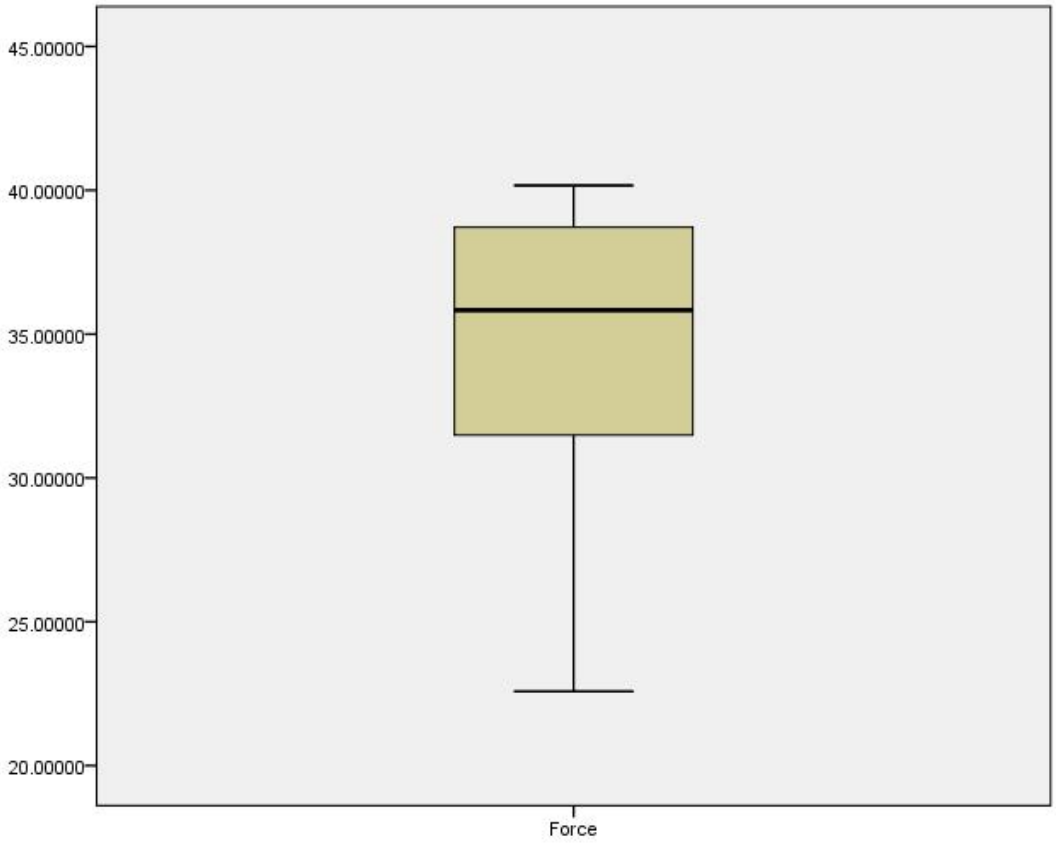

Figure 4.9: Boxplot corresponding to athlete tennis player

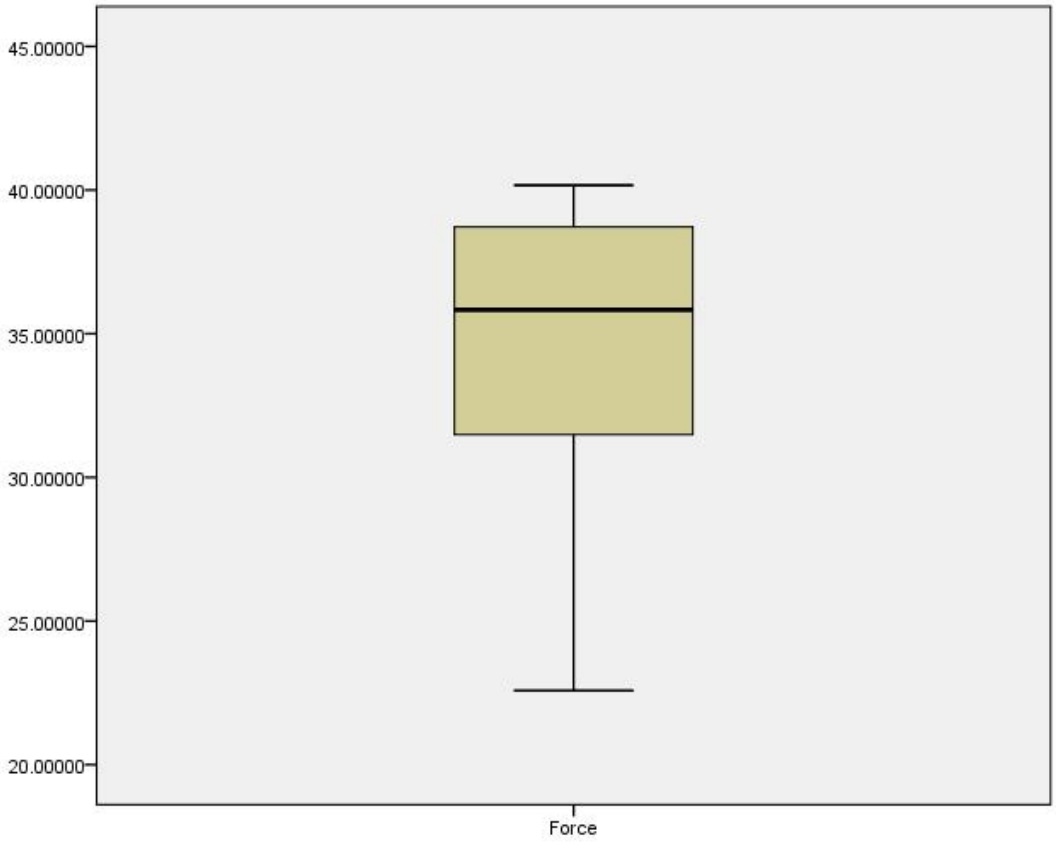

Figure 4.10: Boxplot corresponding to recreational tennis player

The forces as a function of distance from the center of the ball to the strain gauge for the athlete and the recreational players are shown in Figures 4.11 and 4.12, respectively. Each graph shows two potential models (linear and quadratic) that describe the relationship between the ball impact location and the force. The linear trendline was used to fit the increase in force with respect to distance. The second order polynomial was chosen to show the increase and decrease observed in the values of the data with respect to the sweet spot. The force may increase as the ball impact location approaches the sweet spot, then decrease as it passes the center of the racket. The sweet spot is the area of the racket that results in the most powerful hits (30-40 cm from the strain gauge). It was expected that higher peak forces would be found within this area. Therefore, lower peak forces may be observed when the ball is hit outside the sweet spot.

It can be seen in Figures 4.11 and 4.12, that if the ball is hit in the lower region of the racket there is an increase in force as it approaches the region of the sweet spot, and if the ball is hit in the upper region of the racket then there is a decrease in force as the impact moves further away from the sweet spot. The R^2 values in both graphs are quite low indicating that the correlation between distance and force is only loosely related. Although higher order polynomials could have been used to fit the data better and produce better R^2 values, the results would be meaningless with respect to the experiment.

The ball impact location and force for the athlete tennis player are clustered around the same area while the ball impact location and force for the recreational tennis player are more spread out. This difference may be explained by higher skill level players having a more consistent and regular motion throughout the game, hitting the ball within a small area of the racket most of the time.

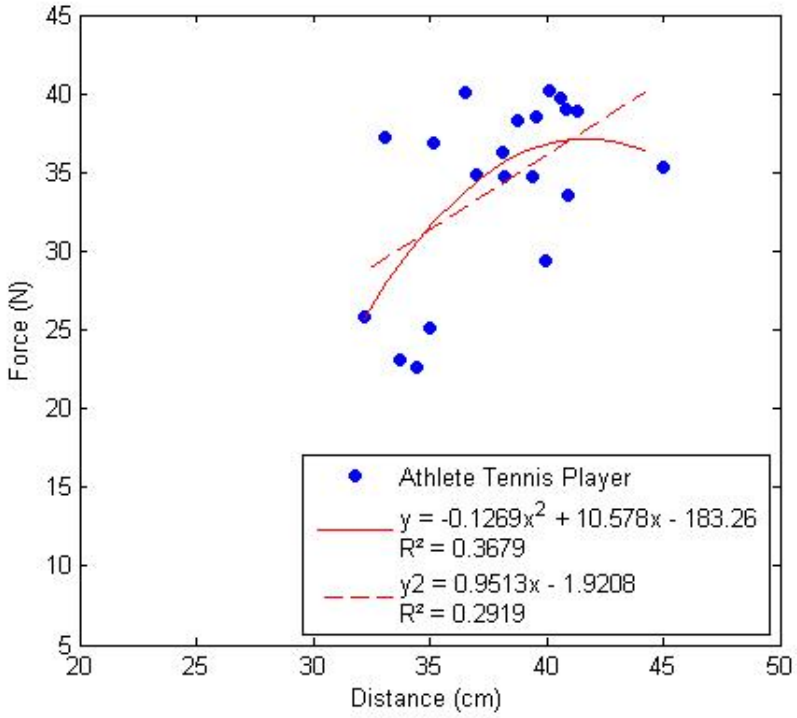

Figure 4.11: Ball forces corresponding to the athlete tennis player

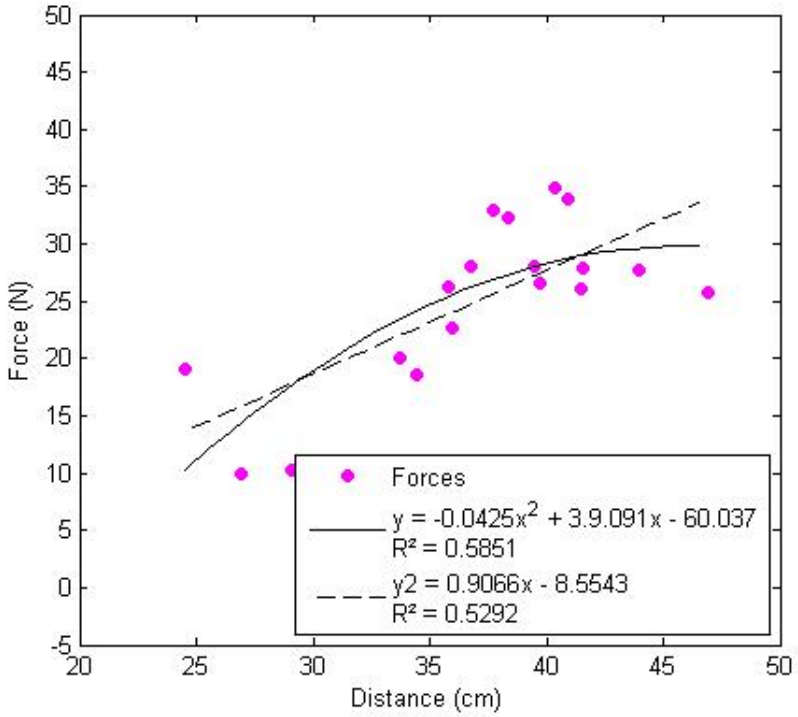

Figure 4.12: Ball forces corresponding to the recreational tennis player

4.6 Interaction Between the Racket and the Ball

To better understand the results, it is necessary to explain that the actual force on the ball is equal to the force observed at the hand plus the transfer of linear and angular momentum. However, the interaction between the racket and the ball was studied as a static system where the wrist reaction forces will be equal in magnitude but opposite in direction to the calculated ball forces. The wrist reaction forces and moments will be closely approximated by the calculated values. The force applied to the racket produces a bending moment at the hand. This bending moment rotates the hand around the fixed y-axis generating a torque (Figure 4.13). Therefore, the torque applied at the wrist is equal to the bending moment at the hand.

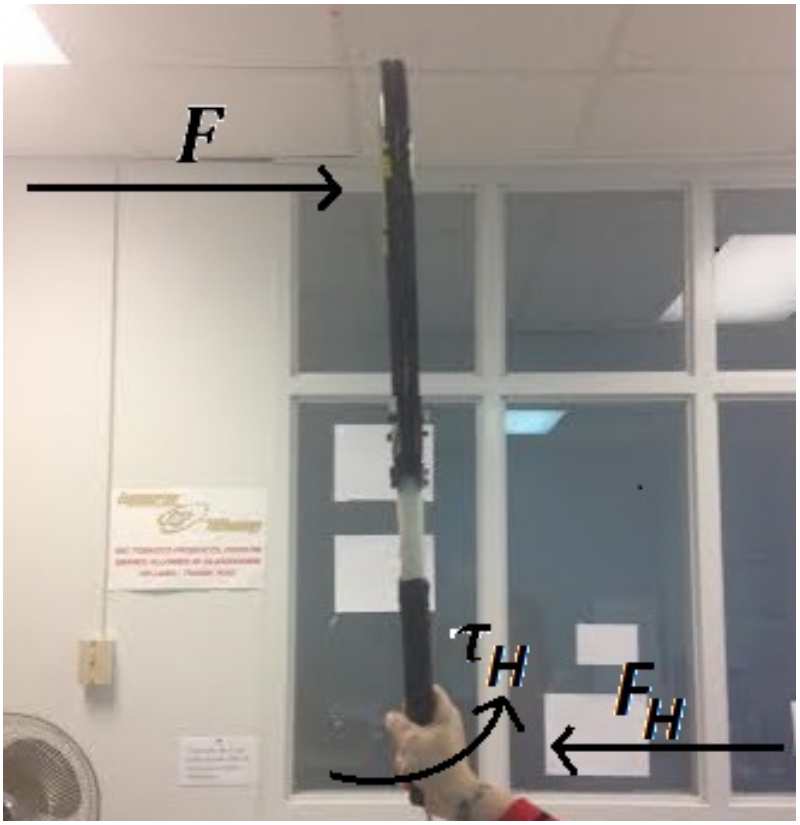

Figure 4.13: Static system formed by the racket and the hand

The wrist reactions forces of both participants combined are shown in Figure 4.14. The mean wrist reaction force of the female athlete tennis player was 34.22 N with a standard deviation of 5.79 N. The recreational tennis player had a mean wrist reaction force of 25.07 N with a standard deviation of 4.47 N. These results show that athlete tennis players wrist reaction forces are higher than recreational tennis players.

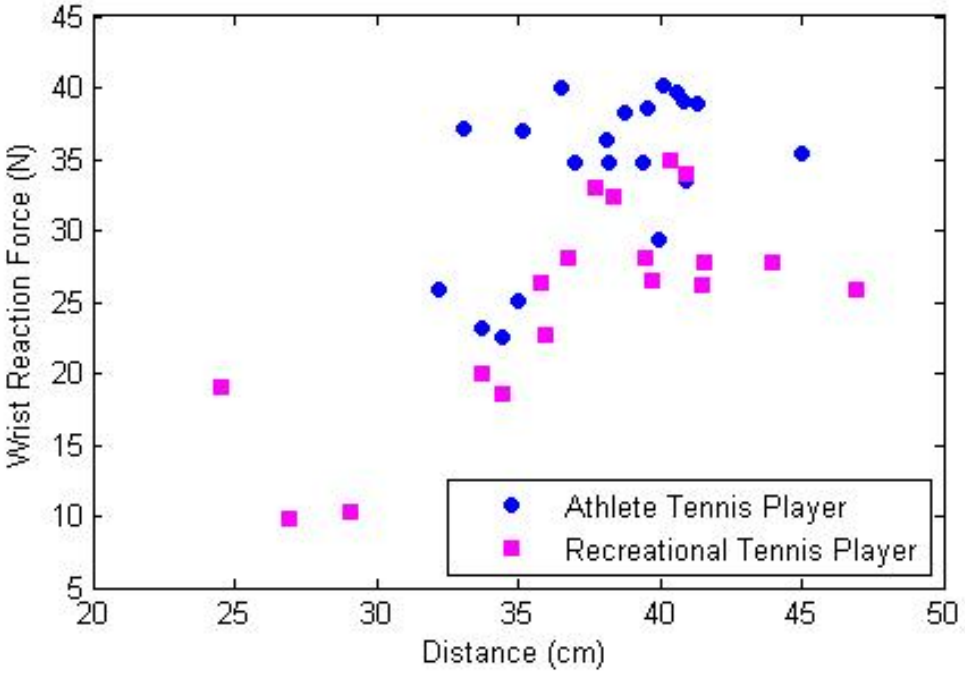

Figure 4.14: Wrist reaction forces of both participants combined

The wrist torques of each participant as well as the torques combined are shown in Figures 4.15 through 4.17. The mean wrist torque for the female athlete was 17.61 Nm with a standard deviation of 3.58 Nm. The male recreational player had a mean wrist torque of 12.89 Nm with a standard deviation of 4.47 Nm. Results show that torques for the athlete tennis player are higher than recreational player torques. Linear and quadratic trendlines were again used to fit the data. It can be seen that the torques increase as the distance increase, but a slight decrease will occur when the location of the ball impact is outside the sweet spot as previously explained.

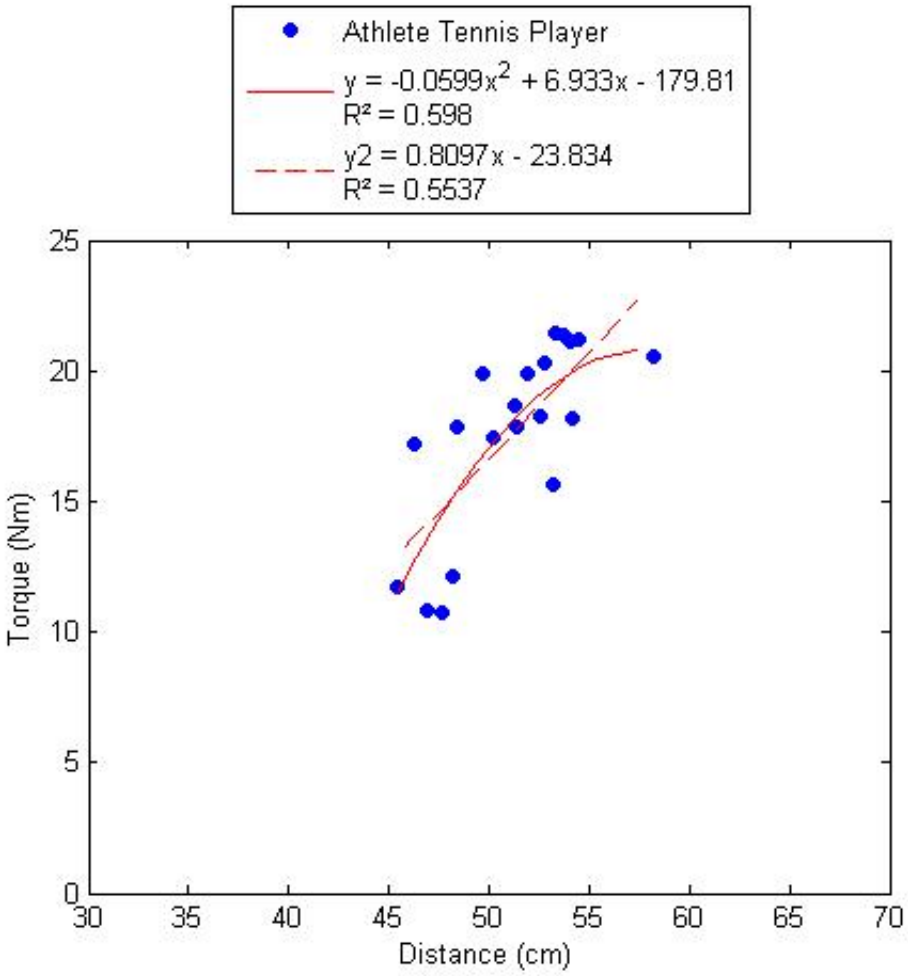

Figure 4.15: Torques corresponding to athlete tennis player

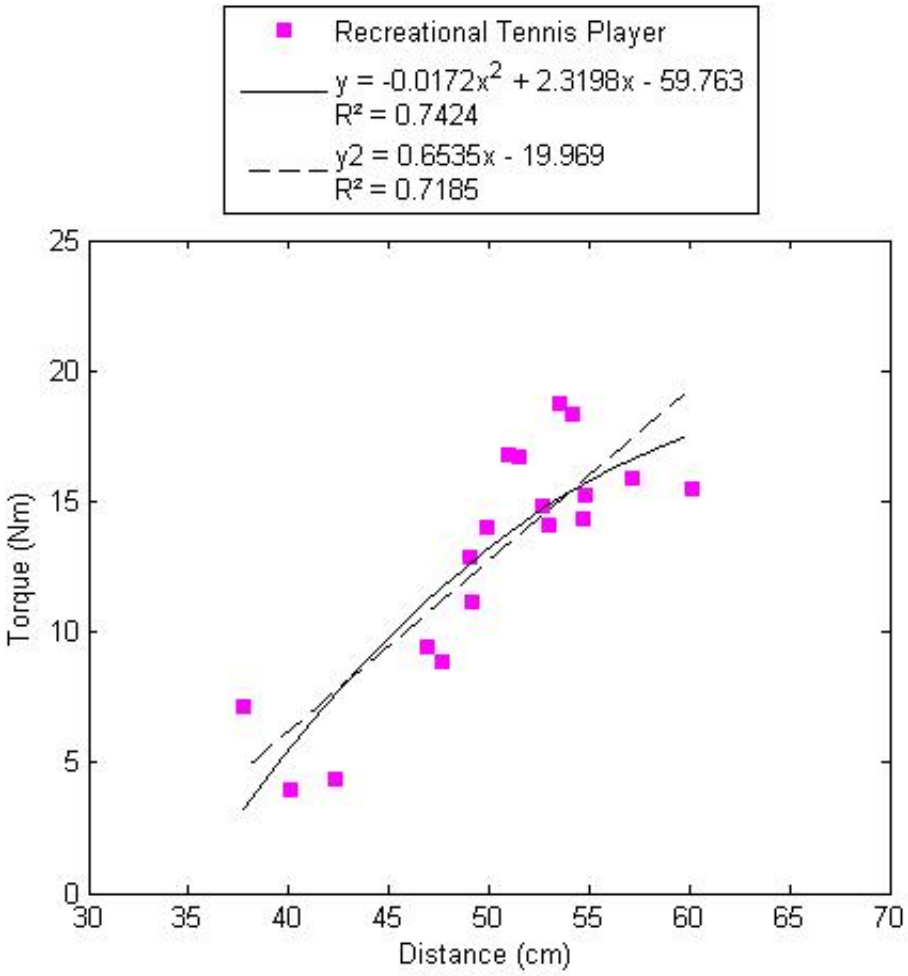

Figure 4.16: Torques corresponding to recreational tennis player

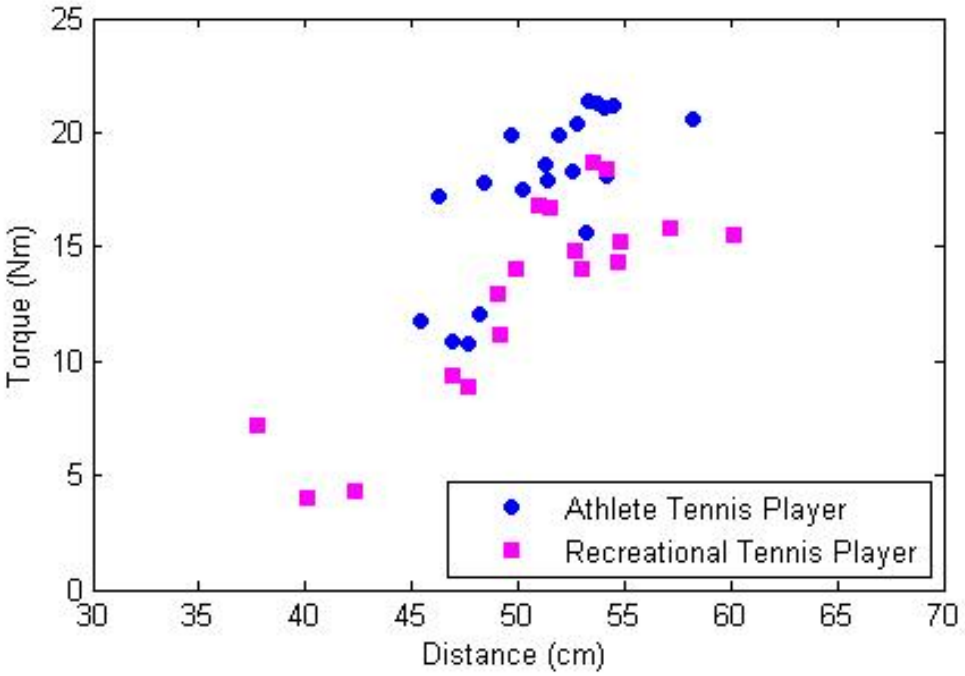

Figure 4.17: Torques of both participants combined

4.7 Frequency of ball impact location with respect to sweet spot

Another way to represent the data is by comparing the ball impact location to the location of the sweet spot. The sweet spot is the area where impact will result in a more powerful hit because the ball absorbs the maximum amount of momentum. The ball impact location for both participants was compared to the sweet using a histogram shown in Figure 4.18. Most of ball impacts by the athlete tennis player fell within the 30-40 cm distance from the strain gauge which corresponds to the location of the sweet spot. Ball impacts by the recreational player were more spread out throughout the racket surface.

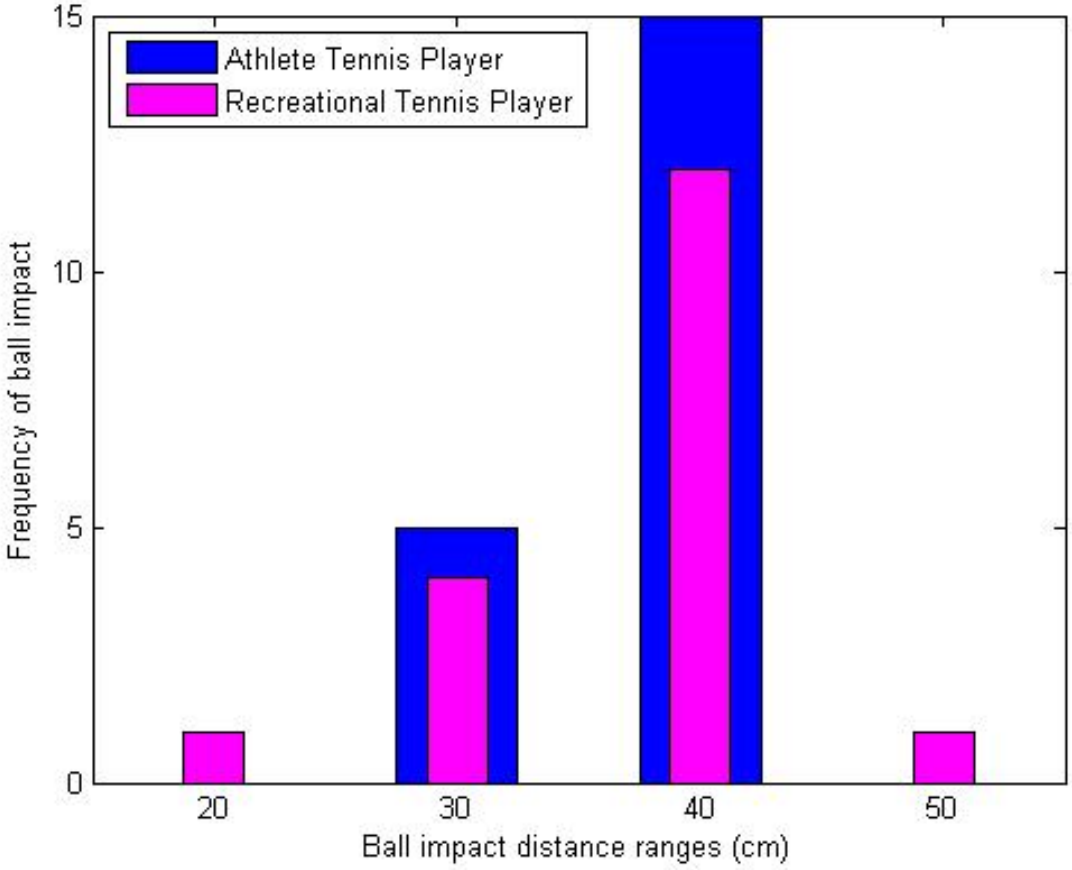

Figure 4.18: Ball impact location of both participants with respect to the sweet spot

4.8 Does Distance Make a Difference in Wrist Reaction Forces?

A statistical analysis was performed to evaluate the effect of distance on wrist reaction forces. An independent-samples t-test (two-sample t-test) was performed to compare the difference in mean force of balls that hit on the upper portion of the racket to balls that hit on the lower portion of the racket. The median of the distances was used to divide the data into the two groups. Descriptive statistics for each group was obtained as well as Levene's test for equality of variances. Equal and unequal variance t-values and a 95% confidence interval for the difference in the means were also calculated. Table 4.5 shows the mean and the standard deviation for the athlete

tennis player.

Table 4.5: Group statistics corresponding to athlete tennis player

Location		N	Mean	Std. Deviation
Force	top	10	36.77	3.43
	bottom	10	31.67	6.68

Prior to performing the analysis, the significance level was set to $\alpha = 0.05$ for the analysis of both participants. Although there are other significance levels to choose from (such as 0.01 or 0.1), it was determined to use the standard level of 0.05.

Lavene's Test for equality of variances shows a significance of $0.002 < 0.05$, therefore, equal variances cannot be assumed (Table 4.6). Then, t-test for equality of means shows that $0.051 > 0.05$, so it was concluded that a significant difference was not present and that the impact location did not significantly affect the wrist reaction force. If the test is repeated with more data point or a wider spread of impact locations is collected, the results may be different.

Table 4.6: Statistical analysis of the athlete tennis player

		Lavene's Test		t-test		
		F	Sig.	t	df	Sig.(2-tailed)
Force	Equal variance assumed	33.492	0.002	2.147	18	0.46
	Equal variance not assumed			2.147	13.432	0.051

A t-test was also performed on recreational tennis player data. Table 4.7 shows the mean and the standard deviation for both groups. In this case, nine data points fell within the top group and nine fell within the bottom group. The mean and the standard deviation are shown for both groups.

Table 4.7: Group statistics corresponding to recreational tennis player

Location		N	Mean	Std. Deviation
Force	top	9	29.27	3.51
	bottom	9	20.87	7.68

Lavene's Test for equality of variances shows a significance of $0.082 > 0.05$, therefore, equal variances can be assumed. Then, t-test for equality of means shows that $p = 0.009$, which is less than $\alpha = 0.05$. Therefore, is was concluded that there was a significant difference in wrist reaction forces for the recreational tennis player serves as shown in Table 4.8.

Table 4.8: Statistical analysis recreational tennis player

		Lavene's Test		t-test		
		F	Sig.	t	df	Sig.(2-tailed)
Force	Equal variance assumed	3.442	0.082	2.986	16	0.009
	Equal variance not assumed			2.986	11.199	0.012

4.9 Results of Ball Velocities

Ball velocities after impact were also evaluated. The approximated ball velocities with respect to ball impact location for both participants are shown in Figure 4.19. Ball velocities corresponding to the athlete tennis player range from 7 to 20 km/h while recreational tennis player ball velocities range from 2 to 17 km/h. Therefore, athlete tennis player velocities tend to be higher. The ball velocity calculated from the ball reaction forces were much lower than expected. Transfer of momentum from the racket to the ball can be used to explain this difference.

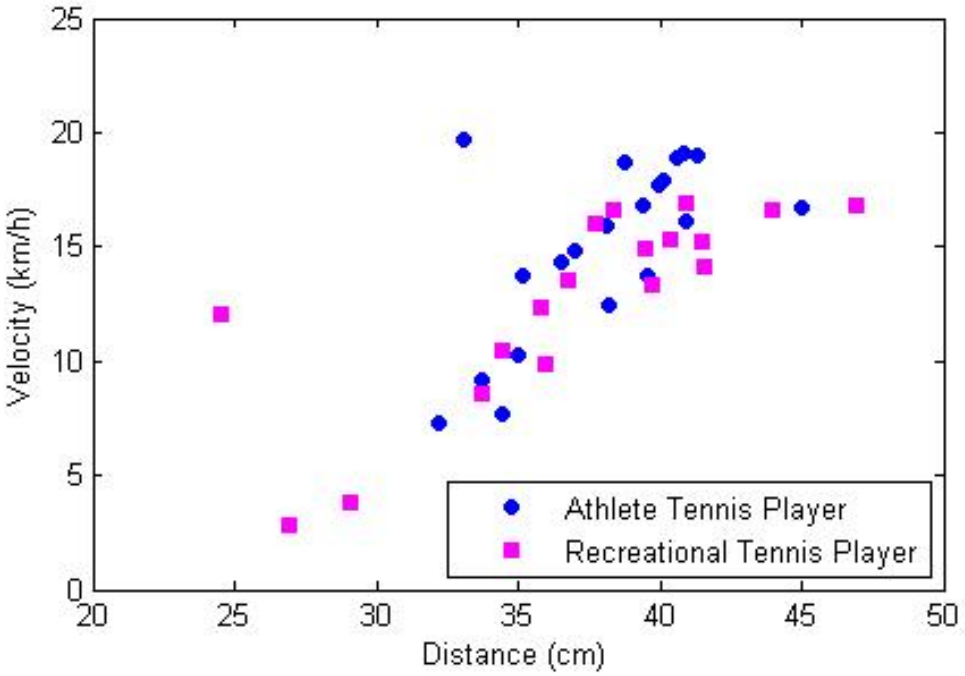

Figure 4.19: Ball velocities of both participants combined

Both participants ball velocities in relation to the peak forces at impact are shown in Figures 4.20 to 4.22 below. A linear trendline is used to fit the data to show that ball velocity increases as ball force increases. This is consistent with what it was previously expected.

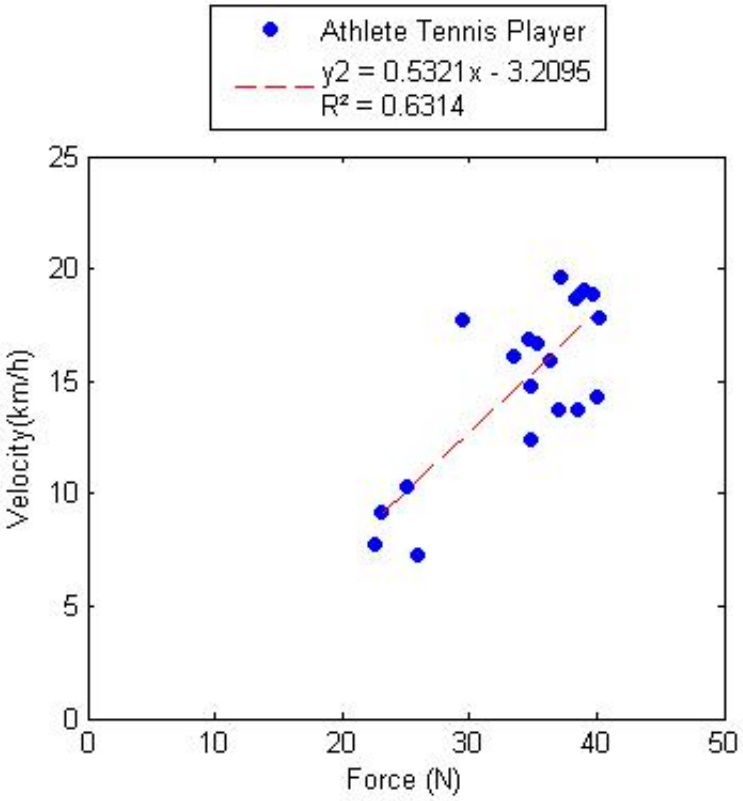

Figure 4.20: Athlete tennis player ball velocity vs. force

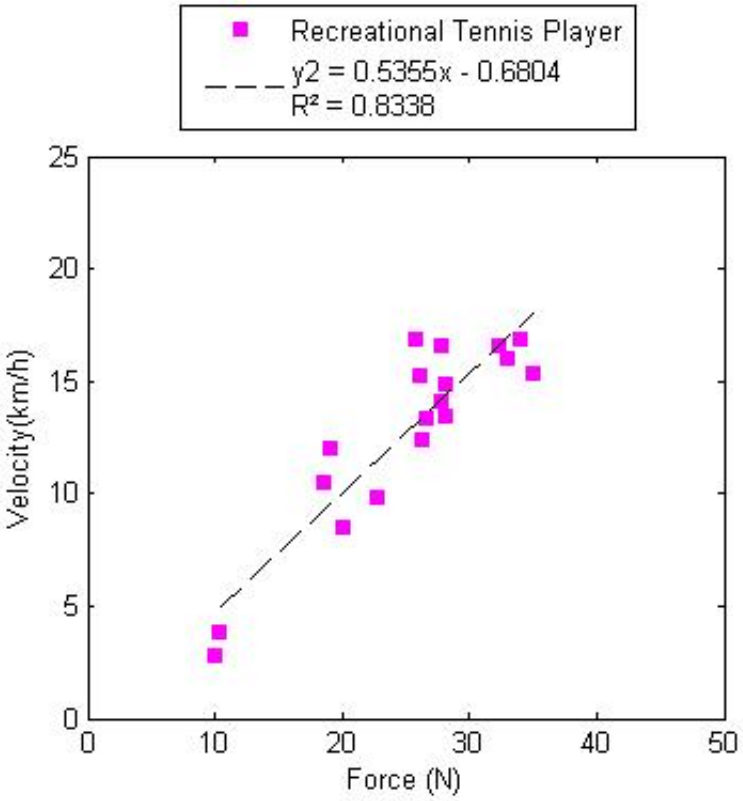

Figure 4.21: Recreational tennis player ball velocity vs. force

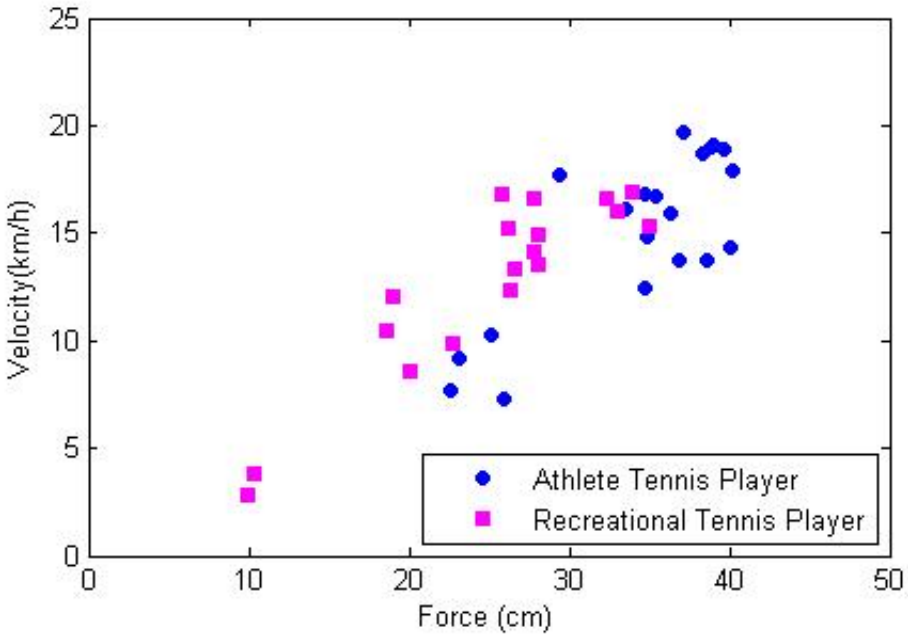

Figure 4.22: Ball velocity vs. force of both participants combined

CHAPTER 5: DISCUSSION AND CONCLUSIONS

In this thesis a new method to evaluate the effect of ball impact location in the overhead motion during game play was presented. An instrumented tennis racket was designed and built to investigate the interaction between the ball and the racket. Results showed that the instrumented tennis racket was able to evaluate the effect of ball impact location of the overhead motion in tennis during game play. The instrumented racket was able to measure ball forces, wrist reaction forces (equal in magnitude to ball forces but opposite in direction as a result of not taking into account the transfer of linear and angular momentums) and torques generated by the bending moments at the hand during ball impact.

Although there were only two subjects, data collected from the testing was consistent with expectations. The difference in skill levels between the athlete tennis player and recreational tennis player was observed when comparing ball velocities, wrist reaction forces, and the ability to control ball impact location. Athlete tennis player's impact locations were closer to one another while recreational tennis player's impact locations were more spread out across the entire string plane. Higher ball forces were observed when the ball was hit within the sweet spot. This allowed maximizing the ball velocities after impact. It was shown that athlete tennis player's velocities were always higher when ball forces were higher. Recreational tennis player's velocities also tend to be higher when peak forces are high but it does not always happen. This proves that players with a higher skill level will have a more consistent and regular motion throughout the game than recreational players. It is more likely that they will hit the same spot in the racket repeatedly which allows maximizing the ball velocity and, therefore, reducing the risks of injuries. More participants will be needed in order to validate the differences observed between test subjects. However, general comments can be made based on the observations. The methods show that

the equipment is capable of collecting this type of data. Furthermore, the analysis methods presented in this thesis can be easily extended to larger test populations.

This device or an improved version may be useful to get a better understanding of the forces and moments created with different types of movements during tennis play. It will be especially useful when employed in collaboration with a motion capture system. A more complete understanding of tennis biomechanics can be gained by including racket impact forces and bending moments with motion capture to quantify the effect that ball impact location has on the transfer of forces to the joints passing through the kinematic chain. In addition, a radar gun could be used to accurately measure the ball velocity. This could be used with the methods developed in this thesis to then determine the portion of the energy transferred to the ball by the wrist force, the portion transferred by liner momentum and the portion transferred by angular momentum.

BIBLIOGRAPHY

[1] P. Kannus, "Etiology and pathophysiology of chronic tendon disorders in sports," *Scandinavian Journal of Medicine and Science in Sports*, vol. 7, no. 2, pp. 78–85, April 1997.

[2] K. Laudner and R. Sipes, "The incidence of shoulder injury among collegiate overhead athletes," *Journal of Intercollegiate Sport*, vol. 2, no. 2, pp. 260–268, December 2009.

[3] A. Cappozzo et. al, "Position and orientation in space of bones during movement: Experimental artifacts," *Clinical Biomechanics*, vol. 11, no. 2, pp. 90–100, December 1996.

[4] N. K. Savage, *Vibration absorption in the tennis grip and the effects on raquet dynamics*, Ph.D. thesis, School of Aerospace, Mechanical and Manufacturin Engineering, RMIT University.

[5] Southern California Orthopedic Institute, "Anatomy of the shoulder," `http://www.scoi.com/shoulder.php`, (accessed Feb 6, 2013).

[6] C. Starkey and J. Ryan, "The shoulder and upper arm," in *Evaluation of Orthopaedic and Athletic Injuries*, J. F. Vilain and M. Foley, Eds., pp. 424–489. F. A. Davis company, Philadelphia, 2nd edition, 2002.

[7] M. Peat, E. Culham, and K. E. Wilk, "Functional anatomy of the shoulder complex," in *The Athelet's Shoulder*, K. E. Wilk, M. M. Reinold, and J. R. Andrews, Eds., pp. 3–16. Churchill Livingstone, Philadelphia, 2nd edition, 2008.

[8] B. Mac, "Anatomy of the shoulder," `http://www.brianmac.co.uk/musrom.htm`, (accessed Feb 8, 2013).

[9] D. Lintner et. al, "Glenohumeral internal rotation deficits in professional pitchers enrolled in an internal rotation stretching program," *American Journal of Sports Medicine*, vol. 35, no. 4, pp. 617–621, April 2007.

[10] van der Hoeven and W. B. Kibler, "Shoulder injuries in tennis players," *British Journal of Sport Medicine*, vol. 40, no. 5, pp. 435–440, May 2006.

[11] T. S. Ellenbecker, E. P. Roetert, and M. Safran, "Shoulder injuries in tennis," in *The Athelete's Shoulder*, K. E. Wilk, M. M. Reinold, and J. R. Andrews, Eds., pp. 429–445. Churchill Livingstone, Philadelphia, second edition, 2008.

[12] C. S. Neer, "Shoulder injuries in tennis players," *Clinical Orthopaedics and Related Research*, , no. 173, pp. 70–77, March 1983.

[13] S. L. Edwards, J. E. Bell, and L. U. Bigliani, "Subacromial impingement," in *The Athlete's Shoulder*. Churchill Livingstone, second edition.

[14] S. J. O'Brien et. al, "The anatomy and histology of the inferior glenohumeral ligament complex of the shoulder," *American Journal of Sports Medicine*, vol. 18, no. 5, pp. 449–456, September.

[15] S. S. Burkhart, C. D. Morgan, and W. B. Kibler, "Current concepts: The disabled throwing shoulder: Spectrum of pathology part i: Pathoanatomy and biomechanics," *Arthroscopy: The Journal of Arthroscopic and Related Surgery*, vol. 19, pp. 404–420.

[16] G. Walch et. al, "Impingement of the deep surface of the supraspinatus tendon on the posterosuperior glenoid rim: An arthroscopic study," *Journal Of Shoulder And Elbow Surgery*, vol. 1, no. 5, pp. 238–245, September 1992.

[17] F. W. Jobe and R. S. Kvitne, "Shoulder pain in the overhand or throwing athlete: The relationship of anterir instability and rotator cuff impingement," *Orthop Rev*, vol. 18, pp. 963–979, 1989.

[18] J. R. Andrews, S. P. Kupferman, and C. J. Dillman, "Labral tears in throwing and racquet sports," *Clinics in Sorts Medicine*, vol. 10, no. 4, pp. 901–911, 10 1991.

[19] V. R. Panossian et. al, "Original article: Biomechanical analysis of isolated type 2 slap lesions and repair," *Journal of Shoulder and Elbow Surgery*, vol. 14, pp. 529–534.

[20] M. R. Safran, "Nerve injury about the shoulder in athletes, part 1: Suprascapular nerve and axillary nerve," *American Journal of Sports Medicine*, vol. 32, no. 3, pp. 803–819, 2004.

[21] S. J. Snyder and J. L. Bond, "Partial articular supraspinatus tendon avulsion (pasta) lesions of the rotator cuff," in *The Athlete's Shoulder*. Churchill Livingstone, second edition.

[22] National Institute of Neurological Disorders and Stroke, "What is thoracic outlet syndrome?," `http://www.ninds.nih.gov/disorders/thoracic/thoracic.htm`, December 28, 2011 (accessed Feb. 6, 2013).

[23] M. R. Safran et. al, "Lower-limb coordination and shoulder joint mechanics in the tennis serve," *Medicine and Science in Sports and Exercise*, vol. 40, no. 2, pp. 308–315, 2008.

[24] C. Martin et. al, "Upper limb joint kinetic analysis during tennis serve: Assessment of competitive level on efficiency and injury risks," *Scandinavian Journal of Medicine and Science in Sports*, vol. 32, no. 3, pp. 803–819, January 2013.

[25] B. Elliott et. al, "Tennis: Technique effects on upper limb loading in the tennis serve," *Journal of Science and Medicine in Sport*, vol. 6, pp. 76–87.

[26] R. E. Bahamonde, "Changes in angular momentum during the tennis serve," *Journal of Sports Sciences*, , no. 8, pp. 579–592, August 2000.

[27] L. H. Wang et. al, "Comparison of segmental linear and angular momentum transfers in two-handed backhand stroke stances for different skill level tennis players," *Journal of Science and Medicine in Sport*, vol. 13, no. 4, pp. 452–459, 2010.

[28] G. D. Abrams et. al, "Review of tennis serve motion analysis and the biomechanics of three serve types with implications for injury," *Sports Biomechanics*, vol. 10, no. 4, pp. 378–390, 2011.

[29] B. J. Gordon and J. Dapena, "Contributions of joint rotations to racquet speed in the tennis serve," *Journal of Sports Sciences*, vol. 24, no. 1, pp. 31–49, 01 2006.

[30] C. Canton-Ferrer, J. R. Casas, and M. Pardas, "Marker-based human motion capture in multiview sequences," *Eurasip Journal on Advances in Signal Processin*, 2010.

[31] M. J. Mathie, J. Basilakis, and B. G. Celler, "A system for monitoring posture and physical activity using accelerometers," in *Engineering in Medicine and Biology Society. Proceedings of the 23rd Annual International Conference of the IEEE*, 2001, vol. 4, pp. 3654–3657.

[32] Inc. Omega Engineering, "What are accelerometers?," `http://www.omega.com/prodinfo/accelerometers.html`, March, 2014 (accessed Dec. 10, 2013).

[33] J. R. Morris, "Accelerometry:a technique for the measurement of human body movements," *Journal of Biomechanics*, vol. 6, no. 6, 11 197.

[34] J. J. Kavanagh and H. B. Menz, "Accelerometry: A technique for quantifying movement patterns during walking," *Gait and Posture*, vol. 28, no. 1, pp. 1–15, July 2008.

[35] A. Ahmadi, D. D. Rowlands, and D. A. James, "Investigating the translational and rotational motion of the swing using accelerometers for athlete skill assessment," *5th IEEE Conference on Sensors*, p. 980, January 2007.

[36] Inc. Omega Engineering, "Introduction to strain gages," `http://www.omega.com/prodinfo/StrainGages.html`, Mar. 2014 Aug. 25, 2013].

[37] National Instruments Coorporation, "Measuring strain strain gages," `http://www.ni.com/white-paper/3642/en/#toc2`, Mar. 2014 (Aug. 25, 2013).

[38] K. Hoffmann, "Applying the wheatstone bridge circuit," `http://www.hbm.com.pl/pdf/w1569.pdf`, (Oct. 10, 2013).

[39] *Instruction Bulletin B-127-14. Strain Gage Installations with M-Bond 200 Adhesive.*